We are IntechOpen, the world's leading publisher of Open Access books
Built by scientists, for scientists

6,900
Open access books available

186,000
International authors and editors

200M
Downloads

Our authors are among the

154
Countries delivered to

TOP 1%
most cited scientists

12.2%
Contributors from top 500 universities

CLARIVATE ANALYTICS
BOOK CITATION INDEX
INDEXED

WEB OF SCIENCE™

Selection of our books indexed in the Book Citation Index in Web of Science™ Core Collection (BKCI)

Interested in publishing with us?
Contact book.department@intechopen.com

Numbers displayed above are based on latest data collected.
For more information visit www.intechopen.com

Chapter 13

Methodology of Thermal Research in Materials Engineering

Anna Biedunkiewicz

Additional information is available at the end of the chapter

http://dx.doi.org/10.5772/51415

1. Introduction

The mechanism of nanostructural carbides synthesis, and chemical activity of nanoparticles in oxidizing environments, even occurring in trace amounts in high-purity gases, require application of precise methods and performing investigations for a wide range of parameters. The methodology of investigation and the way of determination of selected synthesis conditions have been described in this work. Appropriate selection of investigation methodology enables understanding of process mechanisms, performing quantitative analysis and then correct determination of their conditions.

Good basis for analysis of the processes proceeding with participation of solids are kinetic studies. Kinetic studies can be carried out under isothermal or non-isothermal conditions. The transitions with participation of solid reagents usually proceed in many stages. Each step should be treated as an independent process. The measurements indispensable for identification of process stages and reagents are usually carried out by methods of thermal analysis. There are elaborated different methods of kinetic studies. They are the subject of ongoing discussion [1].

Methods of process kinetics are of great significance for materials engineering. In work [2], for example, kinetics of carbothermal synthesis of β-SiC was investigated; in work [3,4] kinetics and mechanism of carbothermal reduction of MoO_3 to Mo_2C; in work [5] kinetics of thermal decomposition of NH_4VO_3; in work [6] kinetics of nanometric ceramic materials synthesis in argon and their oxidation in dry air were investigated.

Kinetic studies of manufacturing process of carbides of the metals, e.g. titanium, vanadium, niobium, tantalum or silicon, are of particular significance. These metal carbides belong to the group of ceramic materials known as conventionally hard materials, high wear and oxidation resistance. This results from the character of chemical bound and crystallographic structure. The fabrication of ultrafine-grain ceramics by powder- metallurgical processes

INTECH
open science | open minds

© 2012 Biedunkiewicz, licensee InTech. This is an open access chapter distributed under the terms of the Creative Commons Attribution License (http://creativecommons.org/licenses/by/3.0), which permits unrestricted use, distribution, and reproduction in any medium, provided the original work is properly cited.

involves a number of serious difficulties. In particular, it is necessary to use ultrafine powders and to optimize sintering conditions so as to prevent grain growth. Due to their high reactivity of such powders, the process must be run in an inert atmosphere. The composites containing nanostructural carbides show higher strengthening in comparison to their microstructural equivalents [7].

Synthesis of these materials is most often carried out by carbothermal reduction of oxides or precursors containing metal-oxygen-carbon conjugation [1,2,8,9,10]. Other attractive synthesis routes are processes of decomposition of organometallic precursors or synthesis carried out with participation of hydrocarbons, eg. CH_4 or C_6H_6, and salts of transition metals [11,12]. Carbothermal synthesis of the carbides proceeds through stages of oxides formation and than oxycarbides formation being the intermediate products of the syntheses. In the latter case the intermediate products are low-stoichiometry carbides of high vacancies concentration resulting from stability range of these phases in equilibrium metal-carbide system.

Presence of oxygen atoms in MC_xO_{1-x} lattice or high concentration of carbon vacancies in MC_{1-x} lattice cause reduction in hardness and wear and oxidation resistance [12,13].

The synthesis stages leading to elimination of above mentioned lattice defects and obtainment of high-stoichiometry, oxygen stripped carbides, characterized by best properties, proceeds in temperature range above 1000ºC.

At the example of decomposition processes investigations process kinetics of the decomposition of NH_4VO_3 has been analysed. The issues concerning kinetics of those processes have been presented at the example of thermal decomposition of NH_4VO_3 to V_2O_5 in dry air. Vanadium carbides, carbonitrides and borides are known ceramic materials [14-16]. NH_4VO_3 could be used in these processes as a precursor. The results of investigations on thermal decomposition of NH_4VO_3 in dry air have been presented. The base of kinetic description of these processes were termoanalytical TG-DSC measurements. They allowed identifying of intermediate and final products, distinguishing stages of the process, determination of their temperature ranges and acquisition the quantitative description. Process kinetics of the stages were described by Kissinger's method, isoconversional method and applying Coats- Redfern equation.

Obtaining the carbides of high carbonization degree, remaining the right grains size and properties, is essential. Selection of parameters meeting these requirements is difficult. Kinetic studies have significance during investigations of conversions proceeding with use of nanomaterials [17]. In the process of TiC synthesis by sol-gel method, described in work [6], the intermediate product is low stoichiometric MC_{1-x} ($x \leq 0.3$). Carbides nucleate and grow in the carbon matrix. The process is carried out in argon. Describing kinetics, Coats-Redfern's equation was applied. Kinetic models of stages were identified basing on statistical evaluation and compliance to a large extent of conversion degrees of stages calculated and determined from termoanalytical measurements. While building the kinetic models of the processes, the results of measurements were treated as statistic values. A system of a complex analysis of measurements results was developed with the use of

artificial neuron networks. Kinetics and by the same, the mechanism of the process of oxidation of nanocrystalline carbides in form of powder were tested, and they were subjected to evaluation based on the comparison of the oxidation rate values.

The possibility to remove the carbon matrix in reaction with oxygen was considered during analysis of the kinetics of the process of TiC_x/C nanocomposite oxidation in dry air. It was proved that it was not possible to purify the obtained nc-TiC by burning in the air the carbon matrix, contained in the system.

2. Thermal decomposition of NH_4VO_3

2.1. Methods kinetic analysis

It is assumed that the rate of non-catalytic, heterophase reactions depends on temperature, conversion degree and pressure

$$r = \frac{d\alpha}{dt} = \phi(T, \alpha, P) \tag{1}$$

After separation of variables we obtain

$$\frac{d\alpha}{dt} = k(T) f(\alpha) h(P) \tag{2}$$

Under thermogravimetric measurements conditions $h(P) \approx 1$ [18]. Then

$$\frac{d\alpha}{dt} = k(T) f(\alpha) \tag{3}$$

Separation of variables means that k(T) function should not depend on conversion degree, and function f(α) should not depend on temperature. Function k(T) is described by Arrhenius equation

$$k(T) = A \exp\left(-\frac{E}{RT}\right) \tag{4}$$

k(T) function maintains its exponential character in relatively narrow range of temperature. Assuming T=0 as integration limit this range is exceeded since k (T) tends asymptotically to the limit values (at $T \to o$ and $T \to \infty$).

By combining (3) and (4) we obtain

$$\frac{d\alpha}{dt} = A \exp\left(-\frac{E}{RT}\right) f(\alpha) \tag{5}$$

Thus, for isothermal conditions we have

$$g(\alpha)=\int_{o}^{\alpha}\frac{d\alpha}{f(\alpha)}=k(T)\mathrm{t} \tag{6}$$

For non-isothermal conditions, at a linear heating rate of sample $\frac{dT}{dt}=\beta$ we obtain

$$g(\alpha)=\frac{A}{\beta}\int_{T\alpha=0}^{T\alpha=1}\exp\left(-\frac{E}{RT}\right)dT \tag{7}$$

The integral has no analytical solution. An important approximate solution is the Coats-Redfern equation [12]

$$\ln\left[\frac{g(\alpha)}{T^2}\right]=F(T)=\ln\left[\frac{AR}{\beta E}\left(1-\frac{2RT_m}{E}\right)\right]-\frac{E}{RT} \tag{8}$$

Based on experimental data for each stage the form of the f(α) or g(α) function most consistent with the experimental data and the parameters of Arrhenius equation A and E should be determined.

During standard thermogravimetric measurements the temperature of the sample, the TG, DTG and HF functions and the mass spectra of evolved gaseous products are recorded. Solid products are identified by XRD method. On this basis the division of the process into stages is made and α(T) dependencies are determined for the stages. The methods of measurement results elaboration and kinetic models recommended by ICTAC Kinetics Comittee are given in work [1]. These include in particular Kissinger's method and isoconversional method.

2.1.1. Kissinger's method

The basis of Kissinger's method are the parameters describing the process rate $\frac{d^2\alpha}{dt^2}=0$. (Tm, αm), determined at different heating rates of samples [14]. For maximum By differentiating equation (5) we obtain

$$\frac{d^2\alpha}{dt^2}=\left\{\frac{E\beta}{RT_m^2}+Af'(\alpha_m)\exp\left[-\frac{E}{RT_m}\right]\right\}\left(\frac{d\alpha}{dt}\right)_m=0 \tag{9}$$

Since $\left(\frac{d\alpha}{dt}\right)_m\neq 0$, therefore

$$\frac{E\beta}{RT_m^2}=-Af'(\alpha_m)\exp\left[-\frac{E}{RT_m}\right] \tag{10}$$

There should be added that the formula (10) requires that $f'(\alpha_m)<0$. In this method therefore only kinetic models fulfilling this condition can be used.

By transforming (10) and adapting the result to the measurements performed at different heating rates of samples the Kissinger equation (11) is obtained

$$\ln\left(\frac{\beta_i}{T_{m,i}^2}\right) = \ln\left[-\frac{AR}{E} f^{'}\left(\alpha_m\right)\right] - \frac{E}{RT_{m,i}} \tag{11}$$

While performing calculations, $\ln\left(\frac{\beta_i}{T_{m,i}^2}\right) \div \frac{1000}{T_{m,i}}$ charts are prepared. Then the activation energy E and the value of expression $\ln\left[-\frac{AR}{E} f^{'}\left(\alpha_m\right)\right] = B$ are calculated by linear regression method.

Knowing B, $-Af^{'}\left(\alpha_m\right)$ is calculated from equation (12)

$$-Af^{'}\left(\alpha\right) = \frac{E}{R}\exp\left(B\right) \tag{12}$$

To calculate A one needs to know the kinetic model for a given stage (form of the function f(α)). The kinetic model most consistent with the experimental data, of the tested models, was established by analyzing the trajectories of Y(T) function depending on α(T). The conversion degrees α(T) for the stages were estimated on the basis of experimental data, whereas the Y(T) function was calculated from the formula

$$Y(T) = \frac{Af'(\alpha_m)}{\beta_i} \int_{T_{\alpha=0}}^{T_{\alpha=1}} \exp[-\frac{E}{RT}]dT \tag{13}$$

For the stage A $f^{'}\left(\alpha_m\right) \approx const.$ The integral was calculated numerically. There should be added that at constant activation energy, trajectories of $\frac{1}{\beta i}\int_{T\alpha=0}^{T\alpha=1} \exp\left[-\frac{E}{RT}\right]dT$ functions depending on the conversion degree, for different β_i, should be the same. The ranges $T_{\alpha=0} \div T_{\alpha=1}$ for given β_i must be determined experimentally. At higher heating rates of the samples there should be wider temperature range $T_{\alpha=0} \div T_{\alpha=1}$. This is consistent with DTG and HF charts. After determining the form of the function f(α) the derivative $f^{'}\left(\alpha_m\right)$ is calculated. Knowing $Af^{'}\left(\alpha_m\right)$ and $f^{'}\left(\alpha_m\right)$ Arrhenius coefficient A is calculated.

2.1.2. Isoconversional method

In the the isoconversional method equation (5), obtained after separation of variables, is also used. Differentiating (5) with respect to ∂T^{-1} we obtain

$$\left[\frac{\partial \ln\left(\frac{d\alpha}{dt}\right)}{\partial T^{-1}}\right]_{\alpha} = \left[\frac{\partial \ln k(T)}{\partial T^{-1}}\right]_{\alpha} + \left[\frac{\partial f(\alpha)}{\partial T^{-1}}\right]_{\alpha} \tag{14}$$

For α = const we have

$$\left[\frac{\partial \ln\left(\frac{d\alpha}{dt}\right)}{\partial T^{-1}}\right]_{\alpha} = -\frac{E_{\alpha}}{R} \tag{15}$$

Integrating (15), taking into account that $\frac{dT}{dt} = \beta$, and generalizing the result for different β_i we obtain

$$\ln\left[\beta_i\left(\frac{d\alpha}{dt}\right)_{\alpha,i}\right] = const - \frac{E_{\alpha}}{RT_{\alpha.i}} \tag{16}$$

Integration constant, according to equation (5), is equal $\ln\left[f(\alpha)A_{\alpha}\right]$. Equation (16) therefore takes the form

$$\ln\left[\beta_i\left(\frac{d\alpha}{dt}\right)_{\alpha,i}\right] = \ln\left[f(\alpha)A_{\alpha}\right] - \frac{E_{\alpha}}{RT_{\alpha,i}} \tag{17}$$

It should be added that the introduction of the coefficients A_{α} and E_{α} depending on conversion degree does not comply with the principle of separation of variables. Equation (17) is used in the differential isoconversional method. The basis of the reaction rate calculations are reaction rates $\left(\frac{d\alpha}{dt}\right)_{\alpha,i}$ determined for selected conversion degrees and different β_i and the corresponding to them temperature values $T_{\alpha,i}$.

In the case of the integral isoconversional method the basis for calculations, for isothermal conditions, is equation

$$g(\alpha) = A\exp\left(-\frac{E}{RT}\right)t \tag{18}$$

Activation energy, in this case, is calculated from the formula

$$\ln t_{\alpha,i} = \ln\left[\frac{g(\alpha)}{A_{\alpha}}\right] + \frac{E_{\alpha}}{RT_{\alpha}} \tag{19}$$

The time of obtaining the assumed conversion degree at different temperatures was designated by $t_{\alpha,i}$. The charts of $\ln t_{\alpha,i} \div \frac{1000}{T_i}$ are constructed. The parameters of equation (19) are calculated by linear regression method. For non-isothermal conditions there is no analytical solution. During the calculations of activation energy there are used approximate equations of general form

$$\ln\left(\frac{\beta_i}{T_{\alpha,i}^B}\right) = const - C\frac{E_\alpha}{RT_\alpha} \tag{20}$$

In this work the Kissinger's-Akoshira-Sunose equation was used

$$\ln\left(\frac{\beta_i}{T_{\alpha,i}^2}\right) = const - \frac{E_\alpha}{RT_\alpha} \tag{21}$$

In this case the charts of $\ln\left(\frac{\beta_i}{T_{\alpha,i}^2}\right) \div \frac{1000}{T\alpha}$ are constructed. The parameters of this equation are calculated by linear regression method.

2.2. Experimental

NH_4VO_3 from Fluka was used as a substrate. Decomposition process was carried out in dry air (Messer, Germany) containing 20,5% vol. O_2 rest N_2. Impurities occurred in amounts: H_2O < 10 vpm, CO_2 < 0,5 vpm, NO_x < 0,1 vpm, hydrocarbons < 0,1 vpm. Thermogravimetric measurements were carried out on TG–DSC Q600 (TA Instruments) apparatus. Gaseous products of proceeding transitions were identified by mass spectrometry method. Pfeifer Vacuum ThermoStar GDS 301 apparatus was used. Solid products were identified by XRD method. X'Pert Pro apparatus from PANalytical with a copper X-ray tube with current voltage 35 kV and intensity 40 mA was used. Spectra processing and analysis was performed using X'Pert HighScore 1.0 software with incorporated ICDD spectra library.

2.3. Results

During the TG-DSC measurements weighed amounts of the sample in the order of 20 mg were used. The temperature of the sample, TG, DTG and HF functions, and mass spectra of gaseous products were registered in time. In all series the temperature of samples changed linearly in time. It was found that thermal decomposition of NH_4VO_3 in dry air proceeds in the three endothermic stages according to

$$6\,NH_4VO_3 \rightarrow (NH_4)_3\,V_6O_{16} \rightarrow (NH_4)_2\,V_6O_{16} \rightarrow V_2O_5 \tag{22}$$

The theoretical, total mass loss of the sample equals 22,29 wt%. The mass losses in the stages, referred to the initial mass of the sample, equal: 11,48 wt% in stage I, 4,404 wt% in stage II, and 6,66 wt% in stage III. The intermediate products (for control also the final product) were obtained under isothermal conditions, in the temperature ranges of their occurrence. As the final product V_2O_5 (ICDD card 85-0601), and as the second intermediate product $(NH_4)_2V_6O_{16}$ (ICDD card 79-205) were obtained. The intermediate product formed in step I was identified on the basis of the mass balance (there is no pattern of this compound in ICDD directory). In all the stages and at different heating rates of the samples evolved: NH_3, H_2O, NO and N_2O resulting from oxidation of NH_3. In the gas phase NO_2 did not occur. The results of this step of research are given in [19].

2.3.1. Analysis of influence of sample heating rate on the course of the process

The influence of sample heating rate on the course of the process was examined on the basis of the TG_u , DTG and HF functions. The measurements were carried out at sample heating rates of: 1; 1,5; 2; 2,5; 3; 3,5; 4; 4,5; 5; 6; 7 ; 8 and 10 K min^{-1}. The isothermal measurements were carried out at the sample heating rate equal to 2 K min^{-1}. Basing on the TG-DSC measurements the division of the process into stages was made and the conversion degrees for the stages were determined. There should be added that the data sets concerning conversion degrees, determined for the stages, are the basis for the description of process kinetics as in [1,17,20-23].

2.3.2. Analysis of TG_u, DTG and HF charts

The trajectories of TG_u, DTG and HF plots are presented in separate figures. In Figure 1 TG_u functions in temperature registered during the measurements are presented.

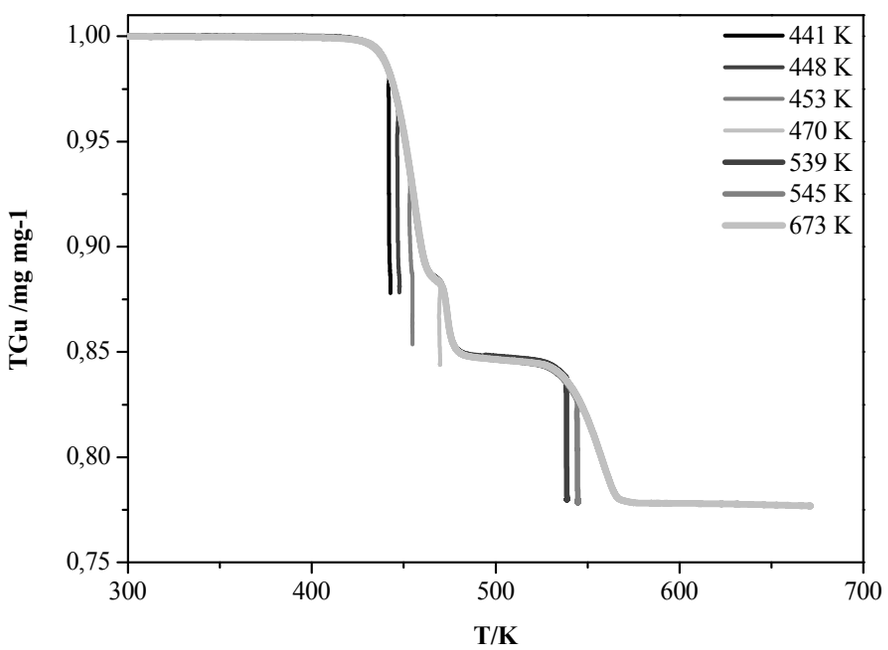

Figure 1. TG_u functions in temperature. Decomposition of NH_4VO_3 in dry air [19].

The linear segments correspond to the isothermal conditions. The samples were heated isothermally until the stable mass has been reached (about 30 min).

In case of the investigated process, under isothermal conditions, the results for the stage could by obtained only at a few temperatures, while at higher temperatures the results were obtained at high conversion degrees. For these reasons, the course of investigated process was not further examined under isothermal conditions.

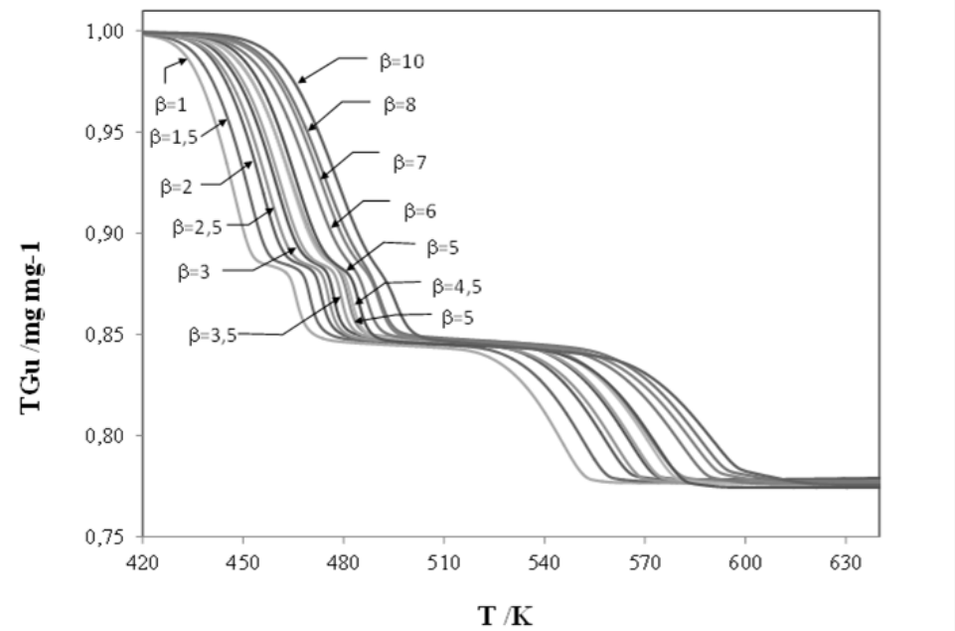

Figure 2. Plot of TG_u functions in temperature. Decomposition of NH_4VO_3 in dry air [19].

In Figure 2 the plots of TG_u function in temperature obtained under non-isothermal conditions are presented. The single curve is formed of about 20 thousand points. The determined TG_u values should depend only on temperature and heating rate of the samples. This was confirmed by neural networks method in reference [24]. All the series were considered simultaneously. The computer software Statistica Neural Network was used. Figure 3 shows an example of DTG plots for selected heating rates of the samples.

It follows that at higher β_i the temperature range $T_{\alpha=0} \div T_{\alpha=1.}$ increases (Fig.3). The temperature range of the process in stage is an important parameter.

Along with the increase of sample heating rates the DTG function plots are shifted into the higher temperature range. It is also visible that at the higher sample heating rates stages I and II are overlapped to a larger extent, and the final segments of plots, corresponding to the stage III, are not monotonic. As mentioned before, this was attributed to the oxidation of formed earlier V_2O_{5-x} to V_2O_5. The T_m temperatures corresponding to peaks of DTG function plots (necessary for Kissinger's method) have been determined. The results are listed in Table 1.

The values of $\alpha_{m,}$ for T_m temperatures given in Table1 were retrieved from data sets of $\alpha(T)$. There are also given the temperature ranges, determined basing on DTG plots, for the stages.

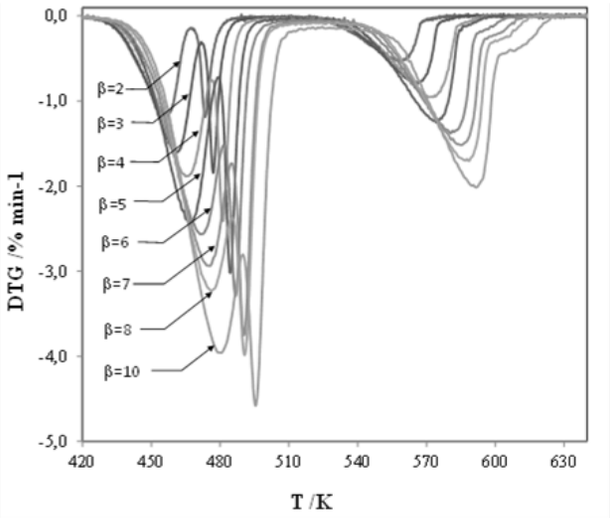

Figure 3. Plots of DTG function in temperature. Decomposition of NH_4VO_3 in dry air [19].

β	Stage I			Stage II			Stage III		
$Kmin^{-1}$	T_m /K	α_m	ΔT /K	T_m /K	α_m	ΔT /K	T_m /K	α_m	ΔT /K
1	447,83	0,721	410,75-457,95	465,65	0,384	457,95-490,65	543,93	0,617	509,25-566,15
1,5	452,62	0,742	405,55-462,85	469,87	0,415	462,85-489,45	550,38	0,653	513,25-572,15
2	457,48	0,761	413,15-467,55	473,58	0,476	467,55-491,35	558,2	0,705	516,25-580,45
2,5	458,06	0,698	412,85-469,65	475,6	0,443	469,65-494,65	560,65	0,701	518,15-583,45
3	460,18	0,683	415,65-472,15	477,16	0,495	472,15-496,15	565,44	0,729	522,95-590,75
3,5	462,25	0,703	415,65-474,15	479,51	0,474	474,15-497,15	567,21	0,737	523,75-590,75
4	465,12	0,689	413,25-476,15	481,41	0,517	476,15-503,15	572,81	0,744	526,55-596,75
4,5	465,32	0,689	417,25-476,95	481,9	0,38	476,95-500,35	572,17	0,743	526,15-595,15
5	467,29	0,714	418,45-479,35				574,3	0,736	530,45-597,95
6	471,44	0,698	416,45-481,85				580,7	0,719	533,45-609,25
7	475,68	0,741	417,15-485,25				588,2	0,83	537,85-614,15
8	476,22	0,71	421,65-485,25				587,06	0,723	536,25-620,75
10	480,09	0,716	423,15-490,15				591,89	0,73	538,85-625,35

Table 1. List of data for Kissinger's method. Thermal decomposition of NH_4VO_3 in dry air.

In Figure 4 the HF function in temperature has been presented for selected example values of β.

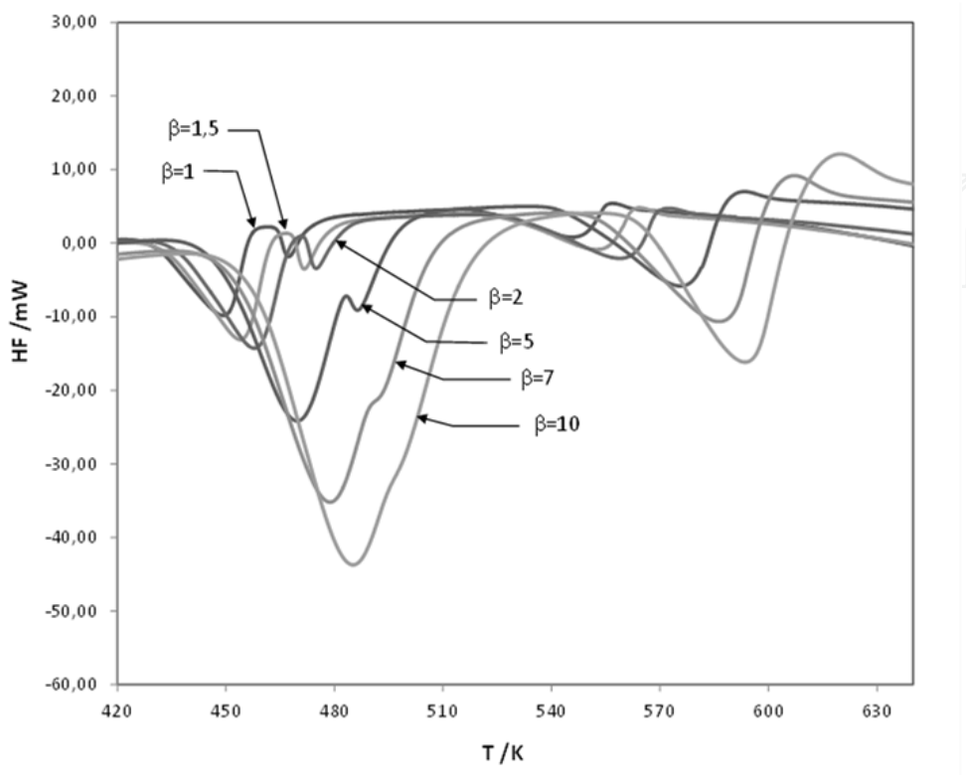

Figure 4. Plots of HF functions in temperature. Decomposition of NH_4VO_3 in dry air.

It is visible from the course of HF plots that in the case there are three endothermic stages referred to the NH_4VO_3 decomposition. The HF plots end with the exothermic transition attributed to the oxidation of small amount of V_2O_{5-x} to V_2O_5. Along with the increase of sample heating rate stages I and II overlap. Peaks of HF function are shifted, with respect to the DTG peaks, by a few degrees into the range of higher temperature. There should be added that NH_3, H_2O, NO and N_2O evolved in all the stages, also at higher simple heating rates.

2.3.3. Analysis of α(T) plots for determined stages

The conversion degrees for stages were calculated from the following formula

$$\alpha(T) = \frac{m_0 - m}{m_0 - m_k} \tag{23}$$

The data concerning the TG_u function were the basis for calculations. During the division of the process into stages also DTG and HF plots were taken into account [22-24].

In Figure 5 the results obtained for the stages are presented. One curve was formed of a few thousand points.

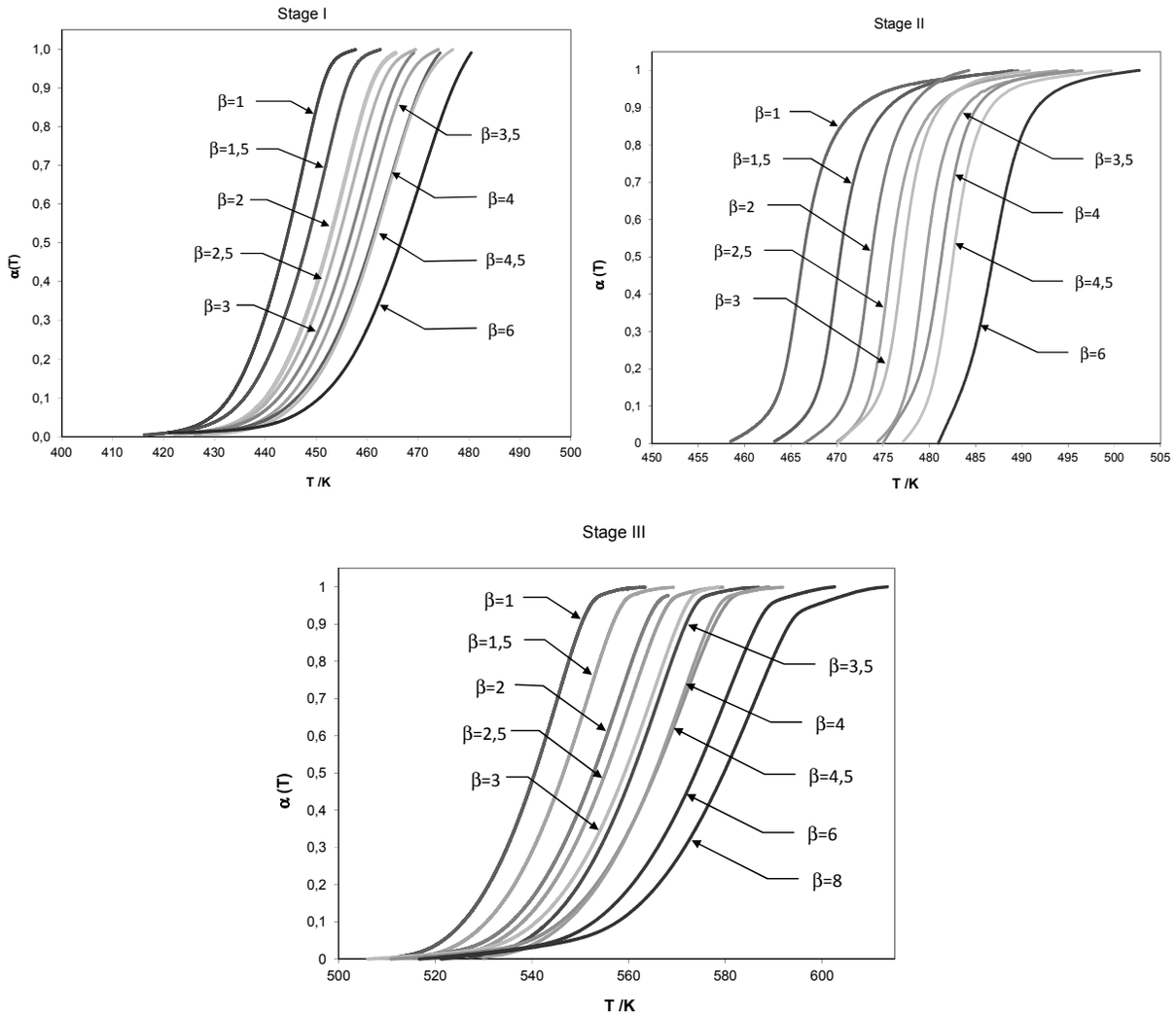

Figure 5. Plots of α(T) depending on temperature for the stages. Thermal decomposition of NH_4VO_3 in dry air.

2.4. Result analysis

2.4.1. Kissinger's method

In Figure 6 the plots of $\ln\left(\frac{\beta_i}{T_{m,i}^2}\right) \div \frac{1000}{T_{m,i}}$ for the stages, obtained on the basis of the data from Table 1, are presented.

The parameters for Kissinger's equation (11) were calculated by linear regression method. The computer software Statistica 6.0 was used. The results are listed in Table 2.

Stage	E kJ mol^{-1}	B*	Af'(α_m) 1 min^{-1}	r_p	model	-f '(α_m)	A 1 min^{-1}
I	117,66	19,496	4,133 E12	0,979	A2	2,476	1,669 E12
II	164,48	30,178	2,37 E17	0,989	A4	6,762	3,504 E16
III	113,75	12,623	4,137 E9	0,985	A2	2,596	1,594 E9

Table 2. List of the results calculated by Kissinger's method. Thermal decomposition of NH_4VO_3 in dry air. * constant in Kissinger's equation (11)

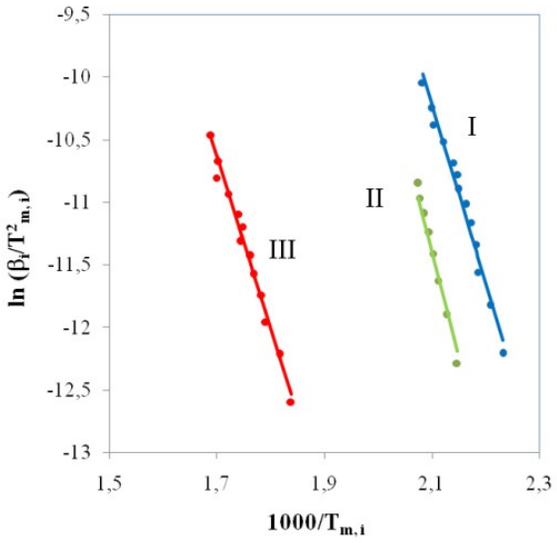

Figure 6. Plots of $\ln\left(\frac{\beta_i}{T_{m,i}^2}\right) \div \frac{1000}{T_{m,i}}$ for the stages. Thermal decomposition of NH_4VO_3 in dry air.

The kinetic models for the stages were determined analyzing the courses of the function

$$Y(T) = \frac{Af'(\alpha_m)}{\beta_i} \int_{T_{\alpha=0,01}}^{T_{\alpha=0,99}} \exp\left(-\frac{E}{RT}\right) dT.$$

There should be added, that the values of α_m determined for the stage, changed marginally for different β. Therefore, there could be assumed that $f'(\alpha_m) \approx const$. In figure 7 plots of Y(T) function for the stages depending on α(T), for β = 3K min^{-1}, are presented as an example.

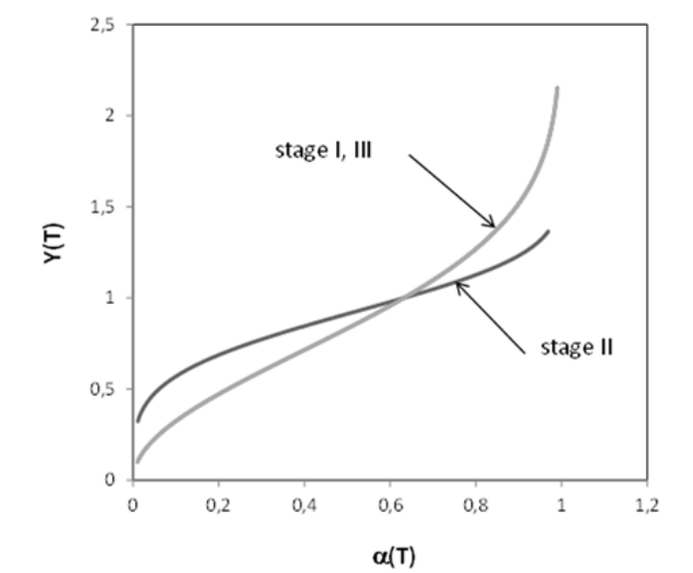

Figure 7. Plots of Y(T) function for the stages depending on α(T) for β = 3K min^{-1}. Thermal decomposition of NH_4VO_3 in dry air.

For the stages I, III the most consistent with experimental data, of the tested models, was the A2 model.

$$g(\alpha)=\left[-\ln(1-\alpha)\right]^{\frac{1}{2}} \tag{24}$$

$$f(\alpha)=2(1-\alpha)\left[-\ln(1-\alpha)\right]^{\frac{1}{2}} \tag{25}$$

$$f'(\alpha_m)=-2\left[-\ln(1-\alpha_m)\right]^{\frac{1}{2}}-\frac{1-\alpha_m}{\alpha_m\left[-\ln(1-\alpha_m)\right]^{\frac{1}{2}}} \tag{26}$$

Whereas for stage II this was the A4 model

$$g(\alpha)=\left[-\ln(1-\alpha)\right]^{\frac{1}{4}} \tag{27}$$

$$f(\alpha)=4(1-\alpha)\left[-\ln(1-\alpha)\right]^{\frac{3}{4}} \tag{28}$$

$$f'(\alpha_m)=-4\left[-\ln(1-\alpha_m)\right]^{\frac{3}{4}}-\frac{3(1-\alpha_m)}{\alpha_m\left[-\ln(1-\alpha_m)\right]^{\frac{1}{4}}} \tag{29}$$

The selection of the model was confirmed making calculations by Coats – Redfern method. The selected models and calculated values of $f'(\alpha_m)$ are given in Table 2.

2.4.2. Isoconversional method

The basis for calculations by this method were dependencies α(T) determined for the stages at different heating rates of the samples (Fig. 5). First, the activation energies were calculated for $\alpha_{m,i}$ corresponding to the inflection points of α(T) curves (average values of α_m given in Table 1). In this case, formula (21) should take the form of equation (11). In Figure 8 the obtained plots of $\ln\left(\frac{\beta_i}{T^2_{\alpha'_m,i}}\right)\div\frac{1000}{T_{\alpha'_m,i}}$ are presented.

The results of calculations are given in Table 3. This method is less accurate than the Kissinger's method

Stage	α_m	E /kJmol^{-1}	B*	r_p
I	0,713	117,3	19,401	0,989
II	0,460	148,2	26,05	0,987
III	0,721	122,3	14,426	0,988

Table 3. List of the results of activation energies calculations by isoconversional method for the inflection points of α(T) curves. *) constant in equation (21).

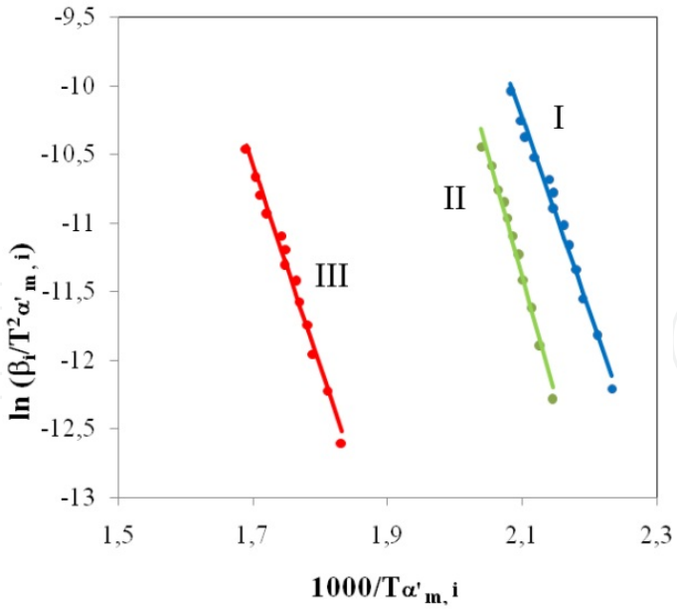

Figure 8. Plots of $\ln\left(\frac{\beta_i}{T^2_{\alpha'_m,i}}\right) \div \frac{1000}{T_{\alpha'_m,i}}$ for the stages. Isoconversional method. Conversion degrees equal to $\alpha_{m,i}$.

The calculations for other values of conversion degree were also performed. Should be noted that α(T) tend asymptotically to the limit values. In these ranges $T_{\alpha,i}$ could not be determined with sufficient accuracy. Therefore, the calculation was performed 0,1<α < 0,90.

The plots of $\ln\left(\frac{\beta_i}{T^2_{\alpha,i}}\right) \div \frac{1000}{T_{\alpha,i}}$ for the stages are shown in Figure 9.

The values of activation energies calculated by the isokinetic method are given in Table 4.

α_i	Stage I			Stage II			Stage III		
	E kJ mol^{-1}	B*	r_p	E kJ mol^{-1}	B*	r_p	E kJ mol^{-1}	B*	r_p
0,1	140,45	27,00	0,986	163,02	30,083	0,996	147,58	21,299	0,991
0,2	131,69	24,303	0,988	161,22	29,493	0,998	137,71	18,709	0,990
0,3	128,45	23,06	0,991	158,71	28,788	0,992	126,45	16,012	0,991
0,4	125,65	22,099	0,995	155,72	27,987	0,994	130,05	16,577	0,989
0,5	123,13	21,256	0,999	156,50	28,187	0,994	127,46	15,849	0,986
0,6	120,29	20,351	0,989	154,54	27,58	0,989	125,48	15,276	0,987
0,7	117,56	19,489	0,988	156,70	28,065	0,985	122,94	14,597	0,985
0,8	114,75	18,61	0,988	158,2	28,365	0,982	121,83	14,227	0,987
0,9	112,38	17,826	0,989				119,92	13,679	0,983

Table 4. The activation energies calculated for the stages by the isoconversional method. Thermal decomposition of NH_4VO_3 in dry air.* constant in equation (21)

In the case of investigated process, the E for the stages I and III (asymmetric plots of DTG and HF), changed continuously along with the change of conversion degree. In the case of stage II (symmetric plots of DTG and HF) E was practically constant, similar to that determined by Kissinger's method. That is the isokinetic method compensates the impact of β_i on the course of the process by changing the activation energy. Theoretically [25] much more interesting is the possibility to compensate the impact of β_i, at a constant activation energy, with use of temperature ranges $T_{\alpha=0} \div T_{\alpha=1}$, the values determined experimentally.

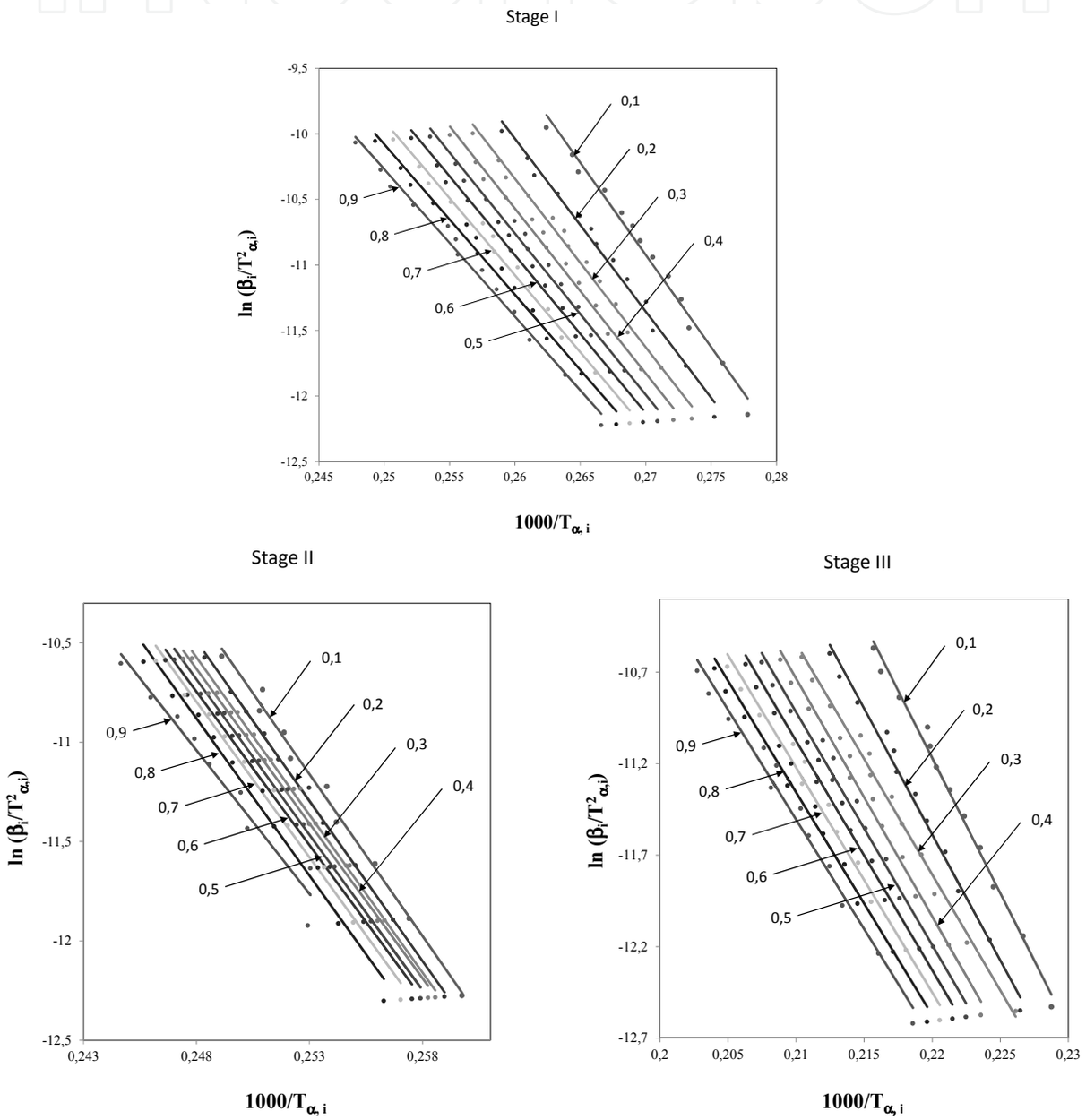

Figure 9. Plots of $\ln\left(\frac{\beta_i}{T^2_{\alpha,i}}\right) \div \frac{1000}{T_{\alpha,i}}$ for the stages. Thermal decomposition of NH_4VO_3 in dry air.

2.4.3. Coats – Redfern method

During the calculations by this method the sets of α(T) presented in Figure 5 were also used.

The activation energies E, determined for the stages by Kissinger's method (for α_m values belonging to the sets of α(T)), were taken as the base values. The plots of $\ln\left[\frac{g(\alpha)}{T^2}\right] \div \frac{E}{RT}$ were constructed. Among the known kinetic models the ones the most consistent with the experimental data were selected; for stages I and III model A2, and for stage II model A4. For the selected model and different β_i the values of the coefficient A were calculated for the stage in the following manner. First Z(T) was calculated from the formula

$$Z(T) = \ln\left[\frac{AR}{\beta E}\left(1 - \frac{2RT_m}{E}\right)\right] = \ln\left[\frac{g(\alpha)}{T^2}\right] + \frac{E}{RT} \tag{30}$$

Then lnA was calculated according to

$$\ln A = Z(T) + \ln\left[\frac{\beta E}{R\left(1 - \frac{2RT_m}{E}\right)}\right] \tag{31}$$

The calculations of Z(T) were performed for the range $0{,}01 \le \alpha \le 0{,}99$. The values of T_m and the temperature ranges for the stages are given in Table 1. However the calculated values of A are given in Table 5. For all the stages the obtained values of coefficient A were higher than the values determined by Kissinger's method. There should be added that the proportion between the values was remained.

Using average values of A the activation energies were tested. The criterion was the best conformity of trajectories of α(T) plots, calculated and determined experimentally, in the whole range. The conversion degrees were calculated as follows. First g(α) was calculated from the formula

$$g(\alpha) = T^2 \exp\left[F(T)\right] \tag{32}$$

Formula (32) is suitable for different models. Whereas the method of calculating conversion degrees depends on the form of kinetic model. For example, for model A2

$$g(\alpha) = \left[-\ln(1-\alpha)\right]^{\frac{1}{2}} \tag{33}$$

thus

$$\alpha = 1 - \exp\left\{-\left[g(\alpha)\right]^2\right\} \tag{34}$$

The values of activation energy calculated in this way are given in Table 5.

β K min^{-1}	Stage I; A2; E=117,66			Stage II; A4; E=164,48			Stage III; A2; E=113,75		
	ΔZ(T)	A E12 min^{-1}	E* kJ mol^{-1}	ΔZ(T)	A E17 min^{-1}	E* kJ mol^{-1}	ΔZ(T)	A E9 min^{-1}	E* kJ mol^{-1}
1	19,81	5,91	114,10	29,98	1,468	157,48	12,72	4,97	110,2
1,5	19,58	7,23	114,36	29,34	1,721	157,85	12,46	5,73	110,5
2	19,22	6,71	114,56	29,31	2,227	-	-	-	-
2,5	19,12	7,61	114,60	28,85	1,436	157,00	12,06	6,52	110,6
3	19,11	9,02	115,06	28,87	2,150	158,20	12,05	7,54	111,1
3,5	18,82	7,85	114,56	28,57	1,860	157,90	11,76	6,70	110,5
4	18,83	9,15	115,26	28,51	1,908	158,50	11,76	7,59	111,5
4,5	18,61	8,27	114,56	28,31	1,845	157,88	11,57	7,10	110,5
5	18,57	8,84	114,76	28,34	2,113	158,80	11,50	7,31	110,6
6	18,41	8,99	115,16	27,98	1,770	158,10	11,33	7,48	111,1
7	18,24	8,85	115,36	27,81	1,742	158,90	11,19	7,56	111,3

Table 5. The kinetic parameters obtained by Coats–Redfern method. Thermal decomposition of NH_4VO_3 in dry air.

The parameters A and E determined by this method for different β_i remain nearly constant.

The corrected activation energies are slightly lower than the ones determined by Kissinger's method; in the case of stage II they are practically equal to the values calculated by isokinetic method. The result is interesting because it shows that the activation energy determined by Kissinger's method can be regarded as representative for the whole set of α(T) related to the stage. It should also be emphasized that determining the triad of g(α), A and E directly from the Coats-Redfern equation, usually the good results are not obtained [1,21,24]. That is it is a matter of calculation methods, and not of the Coats-Redfern equation.

Using the kinetic parameters given in table 5 the verifying calculations were performed. For the selected β_i the trajectories of α(T) and r(α,T) functions were determined. The process rate was calculated from the formula

$$r(\alpha,T) = A\exp\left(-\frac{E}{RT}\right)f(\alpha) \tag{35}$$

While calculating f(α) the values of α(T) obtained from the Coats-Redfern equation (formulas (32)–(34)) were used. In Figure 10 the results obtained for stage I and II (β= 2, 4 and 6 K min^{-1}) are presented as an example.

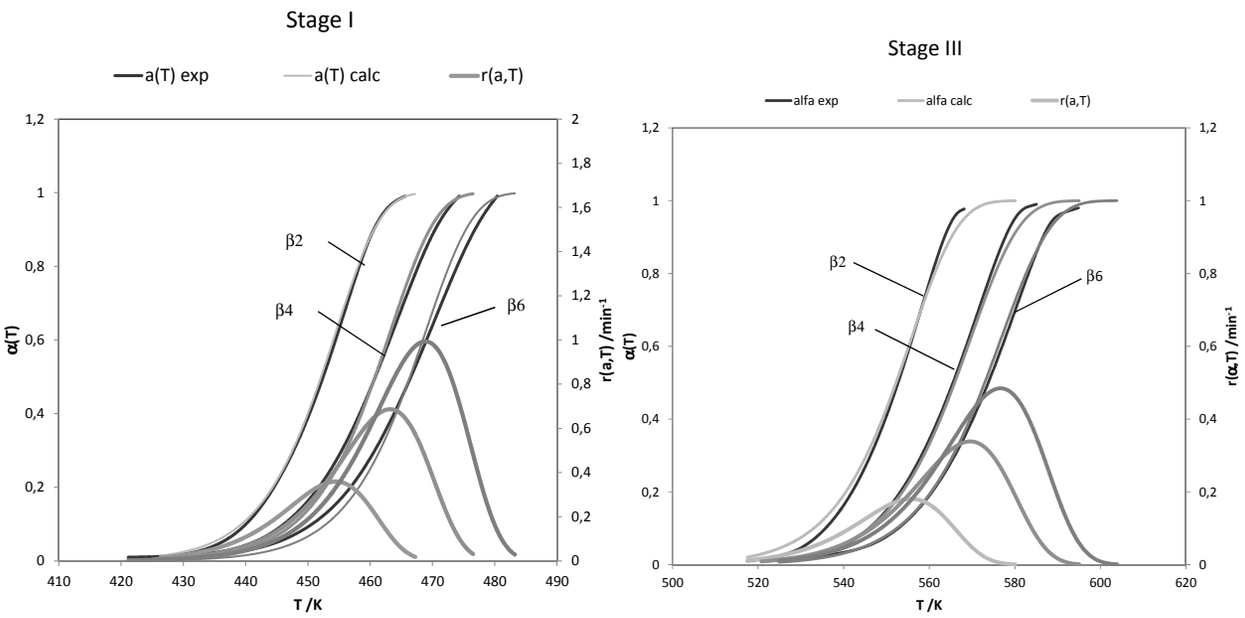

Figure 10. Plots of α(T) and r(T, α) for the stage I and III. Thermal decomposition of NH_4VO_3 in dry air.

The results are fairly well consistent with the experimental data; at the experimentally determined temperature ranges the process rates change from zero for α(T) = 0, reaching the maximum values at the points of inflection of α(T) curves, and then decrease to zero at $\alpha(T) \to 0$. The obtained results show that in our study Coats-Redfern equation was of great importance. Due to the analytical form it is also easy to use in the calculations of the kinetics of heterophase non-catalytic processes.

3. Heat treatment of TiCx/C. Carbonisation of nc-TiCx

Manufacturing, storage and use of nc-TiC in form of powder for sintering or co-deposition processes involves the possibility of occurrence of free carbon in the system. Carbon can be a by-product of the synthesis process (pyrolysis of hydrocarbons) and remain in equilibrium in the TiC-C system or be the product of oxidation of TiC in the air according to the mechanism proposed by Schimada [26], whereby the oxygen dissolves in the carbide and the layer containing oxycarbides is formed.

$$TiC + (3/2)\ x\ O_2 \rightarrow TiC_{1-x}O_x + CO_2 \tag{36}$$

In second stage, in the layer amorphous TiO_2 is formed and elemental carbon is produced [27-31]

$$TiC_{1-x}O_x + (1 - x/2)\ O_2 \rightarrow TiO_2 + (1 - x)C \tag{37}$$

The produced carbon changes the state of the surface of TiC particles. A low oxygen content is the most important prerequisite for high sintering activity of the nanocrystalline TiC powders, especially in the sintering processes, synthesis of the nanocomposites for example nc-TiC in metallic matrices.

In the manufacturing of nanomaterials by sol-gel method the second, high temperature, i.e. at temperatures above 1400 K, stage is essential. The first stage of this method is the sol-gel technique. This stage is carried out at lower temperature. The intermediate product of pyrolytic decomposition of PAN-DMF-$TiCl_3$ is formed - the powder containing nanocrystalline TiCx in carbon matrix [6]. Nanocrystallites of titanium carbide are characterized by high fraction of lattice defects, i.e., vacant carbon sites, presence of oxygen and/or nitrogen. In the second stage carbonisation and purification of TiC_x/C composite in argon takes place. It is essential to obtain the materials with high values of the C/Ti ratio, while maintaining the proper, nanometric grain size, in order to obtain the most favourable properties such as hardness and oxidation resistance. The selection of parameters meeting these requirements is difficult.

There was assumed that the good basis are kinetic studies. They allow to determine the intermediate and final products, distinguish the stages of the process, determine the temperature ranges of their courses and obtain a quantitative description.

The kinetic measurements were carried out using TG-DSC-MS technique. Nanoparticles size, lattice parameter, chemical and phase composition before and after heat-treatment were determined with the following techniques: XRD (Philips PW3040/x0 X'Pert Pro), HRTEM (JEM 3010), SEM (JEOL JSM 6100), EDX (Oxford Instruments, ISIS 300), XPS (SIA 100 Cameca), total carbon measurement (MULTI EA2000, AnalyticJena), and the presence of free carbon was estimated by Raman Spectroscopy. The measurements were carried out under non-isothermal and isothermal conditions. The advantage of this method is the possibility of continuous registration of measured values and use of small weighed amounts of samples during measurements. The procedure is illustrated at the example of heat treatment in argon of the nanocomposite powder containing nc-TiC_x ($x \leq 0.7$) in carbon matrix obtained by sol-gel method. The method ensures maintaining the small size of crystallites, by physically limiting the volume available for their growth, and the matrix prevents agglomeration of particles and oxidation during storage and transport.

At a certain temperature range, and under certain conditions, the reaction of carbonisation is possible

$$TiC_x + yC \rightarrow TiC_{x+y} \tag{38}$$

Heating of the samples in an argon atmosphere can lead to the growth of crystallites. The aim of this study was to develop conditions for annealing of the composite, under which, as a result of carbonisation, TiC_x reaches a high stoichiometric composition, i.e. $x > 0.8$, at the minimal growth of crystallites. Obtaining such optimal material properties can be controlled by selecting the appropriate temperature and rate of the process.

The thermogravimetric measurements were carried out at sample heating rates of 10, 20, and 50 $Kmin^{-1}$. The mass of the samples were ca. 40 mg. During the measurements the samples were heated up to 1473, 1573, 1673 and 1773 K. These temperature values correspond to the isothermal conditions. The samples were heated under isothermal

conditions for 6 h. High-purity argon 'Alphagaz 2 Ar' from Air Liquide (H_2O\ppm/mol, O_2\0.1 ppm/mol, C_nH_m\0.1 ppm/ mol, CO\0.1 ppm/mol, CO_2\0.1 ppm/mol, H_2\0.1 ppm/mol) was used during experiments. With regard to reactivity of O_2 the special attention during measurements was given to possibility of oxidation of components of the system during the process run. Argon purge flow rate during measurements was set at 100 cm^3/min. The part of the results in works [17,32] were presented. Below the complete analysis description were introduced.

3.1. Kinetic analysis

The kinetic description of the process was based of thermogravimetric measurements. The results of the measurements are presented on the plots of sample temperature, TG, DTG and HF function dependencies on time (Fig. 11).

Initially the measurements were carried out under non-isothermal conditions at a linear change in sample temperature, then at the transitional regime, and finally under isothermal conditions (Fig.11a). It should be added that these results were the basis of the description of the process. The theory of kinetics under non-isothermal conditions require that this function depends only on the sample heating rate and temperature. The results were evaluated by neural networks method. Neural networks, used to analyze the non-isothermal measurements, were previously described in [20-23]. The TG_u function was the described (dependent) variable, and the sample heating rate and temperature were the describing (indepedent) variables. All the measurement series were examined simultaneously. The received network was GRNN 2/11310. Statistical analysis of this network is given in Table 6.

Parameter	Tr	Ve	Te
S.D. Ratio	0.01716	0.01926	0.01734
Correlation	0.999874	0.999845	0.99987

Table 6. Statistical estimation of GRNN 2/11310 network

In columns 2, 3, 4 the statistical evaluation of training (Tr), verification (Ve) and testing (Te) subset is listed.

A high accuracy was obtained. The TG dependencies determined experimentally could have been used in kinetic calculations.

The essential operation is the division of the process into stages. Basing on the presented measurement results four stages of the process were identified (Fig. 12). In the endothermic stage I, proceeding with a weight loss, the release and desorption of volatile products, contained in the samples after the first stage, occurred. In the exothermic, second stage, marked with the symbol II, proceeding with a samples weight gain, the oxidation of non-carbonised nc-TiC_x/C by oxygen present in trace amounts in argon occurred. In the endothermic third stage, labeled by III, simultaneously proceeded the pyrolysis of organic

admixtures and carbonisation of nc-TiC_x/C. The pyrolysis and carbonisation were treated as concurrent reactions. Stage IV (exothermic) proceeded with sample weight gain. It concerns the oxidation of carbonised nc-TiC with oxygen contained in argon. The process proceeded at temperature above 1573 K.

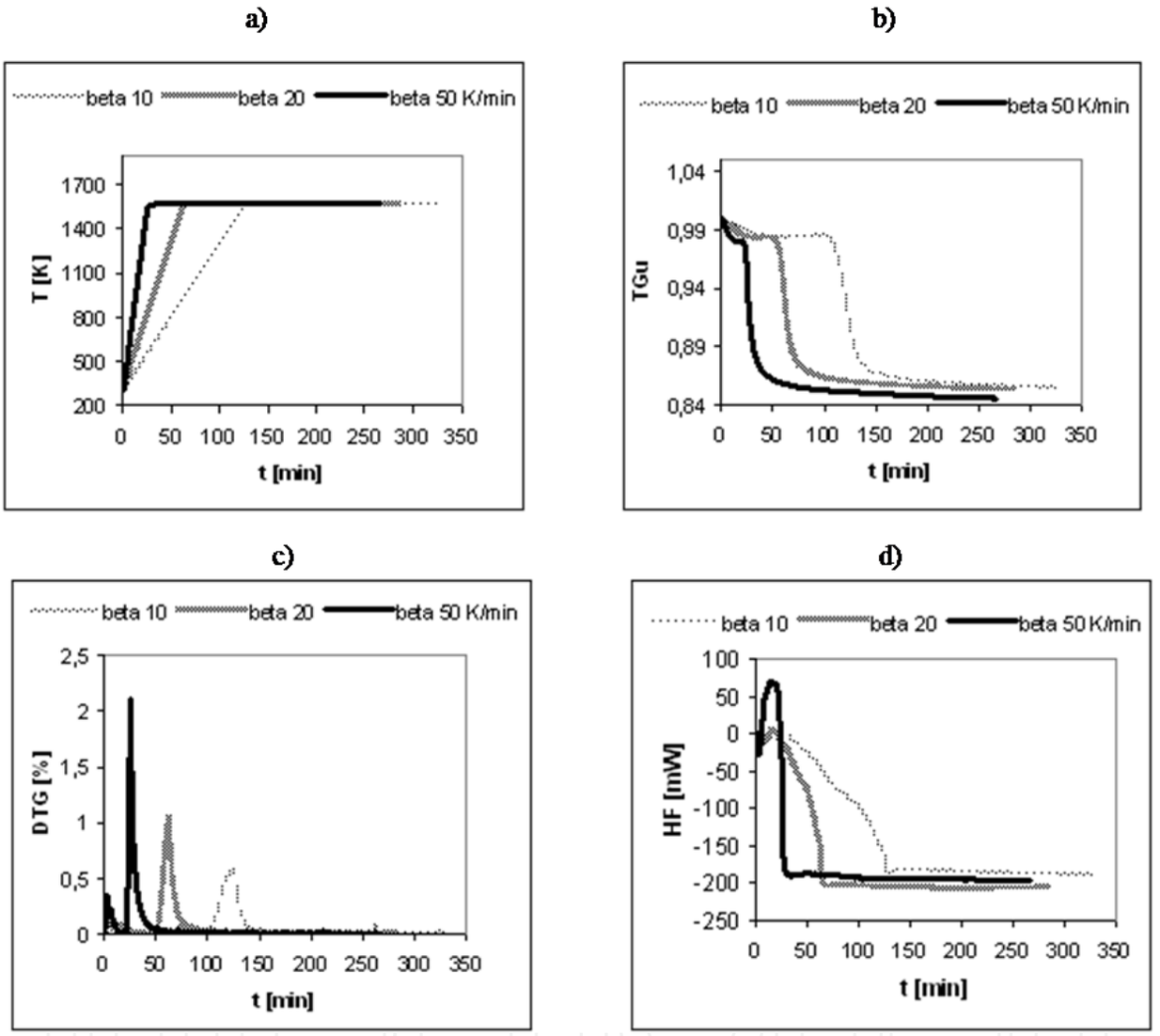

Figure 11. Plots of T, normalized TG function and DTG and HF in time. Heat treatment of nc-TiC/C in argon. a) temperature, b) normalized TG, c) DTG, d) HF

During the thermogravimetric measurements the evolved gaseous products were identified by mass spectrometry method. The compounds produced in the reaction with the oxygen present in trace amounts in argon, are described in detail, because these processes could affect the quality of the obtained, carbonised nc-TiC. CO_2-m/e44, CO-m/e28 NO-m/e30 and NH_3-m/e17 have been identified. NH_3 formed as a result of pyrolytic decomposition of carbon compounds was the precursor of nitric oxide. CO_2-m/e44 mass spectrum, is shown in Figure 13 as an example. To facilitate the analysis of the results the normalized TG_u function is also plotted.

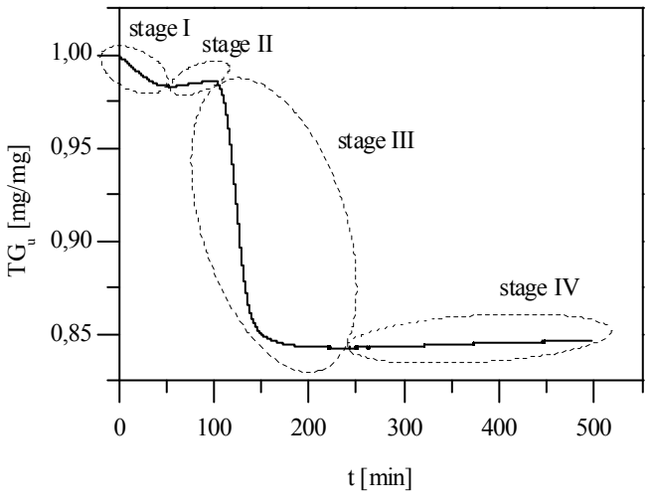

Figure 12. Plots of normalized TG functions in time for β=10 K/min and 6h at 1673 K recorded during the heating of nc- TiC_x/C in argon.

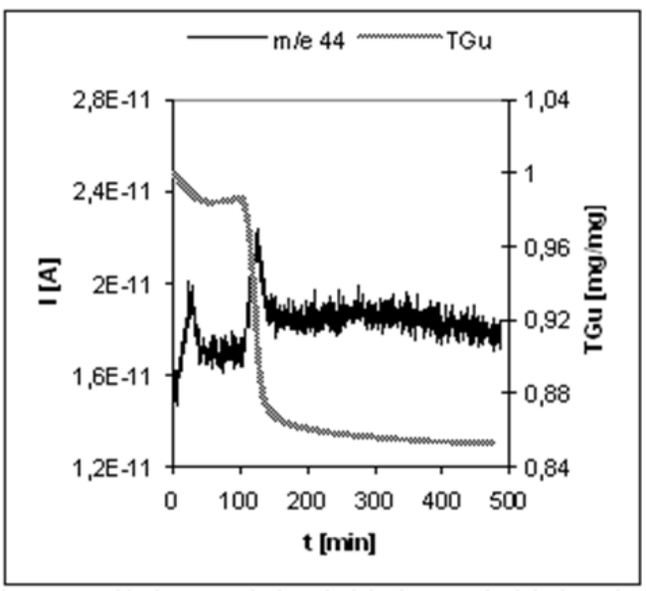

Figure 13. Mass spectra of CO_2 and normalized TG function plots. Heat treatment of nc-TiC/C in argon at the heating rate 10 $Kmin^{-1}$.

The analysis of mass spectra allowed the more accurate characterisation of distinguished stages. In stage I volatile products were evolved. CO_2, CO and NO were also formed. In this stage H_2, NH_3, HCN and CH_3–CH_3, CH_2=CH_2 and CH≡CH also evolved. In stage II oxidation of non-carbonised nc-TiC_x/C occurred. During the course of stage III CO and CO_2 were emitted. They were attributed to the oxidation of released hydrocarbons. HCN, CH_3–CH_3, CH_2=CH_2, and CH≡CH were also formed.

The correct kinetic description was hindered by evolution of secondary products. Therefore the values of α(T) determined for each stage required an independent evaluation.

3.2. The results of calculations

For distinguished stages, basing on the TG function, the conversion degree was calculated. The formula (23) was used.

During the measurements weight changes of the samples were as follows: in stage I: 10 $Kmin^{-1}$ (1.6%), 20 $Kmin^{-1}$ (1.7%) and 50 $Kmin^{-1}$ (2%). In stage II, the sample weight changes equaled: 10 $Kmin^{-1}$ (0.089%), 20 $Kmin^{-1}$ (0.047%). Whereas in whole the range of the course of stage III weight changes were: 10 $Kmin^{-1}$ (13.47%), 20 $Kmin^{-1}$ (13.23%) and 50 $Kmin^{-1}$ (13.66%). The obtained relations of α(T) for stages I and II are shown in Figure 14.

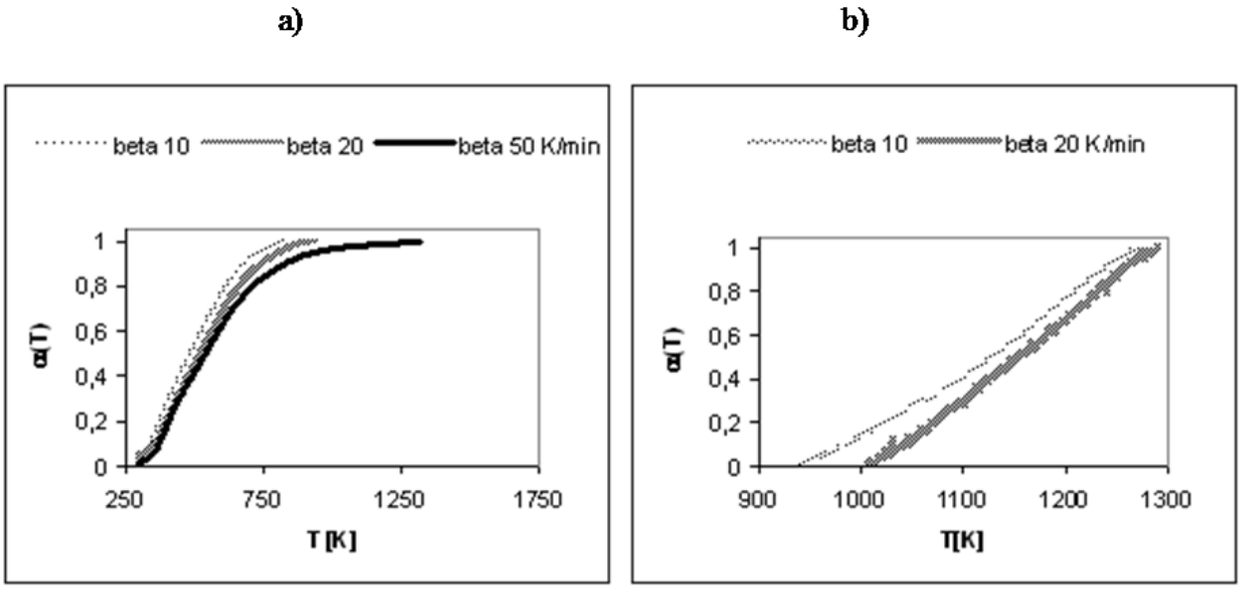

Figure 14. Temperature dependencies of α(T) function; a) stage I, b) stage II.

In accordance with the theory of kinetics of heterogeneous processes the plots of α(T) are shifted into higher temperature range along with the increase in samples heating rate.

Due to the measurements in different regimes the dependencies of α(T) determined for stage III required a more detailed discussion. The conversion degree in stage III was changing regularly in time (Fig. 15a). Irregular changes were observed in the trajectories of the curves of conversion degree dependencies on temperature (Fig. 15b). It was also found that in the transient area a significant increase in conversion degree took place.

The results presented in Figure 16a were elaborated according to the rules of non-isothermal processes theory and in Figure 16b according to the isothermal processes theory.

The plots of α(T) determined for non-isothermal conditions concern the pyrolysis process.

At low temperatures, there is no carbonisation of nc-TiC, and at temperature above 1573 K pyrolysis proceeded much faster than carbonisation. Under the non-isothermal conditions, the transition from one temperature range to the other was short. As a result the influence of carbonisation on the recorded samples weight loss was not revealed.

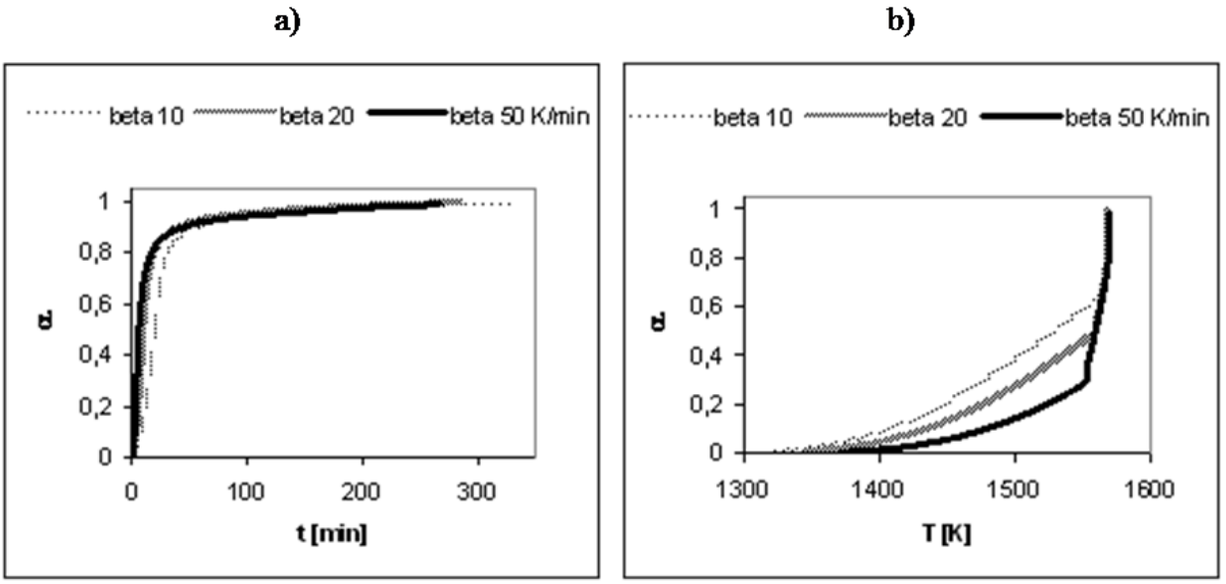

Figure 15. Total conversion degree. Stage III; a) time dependency b) temperature dependency.

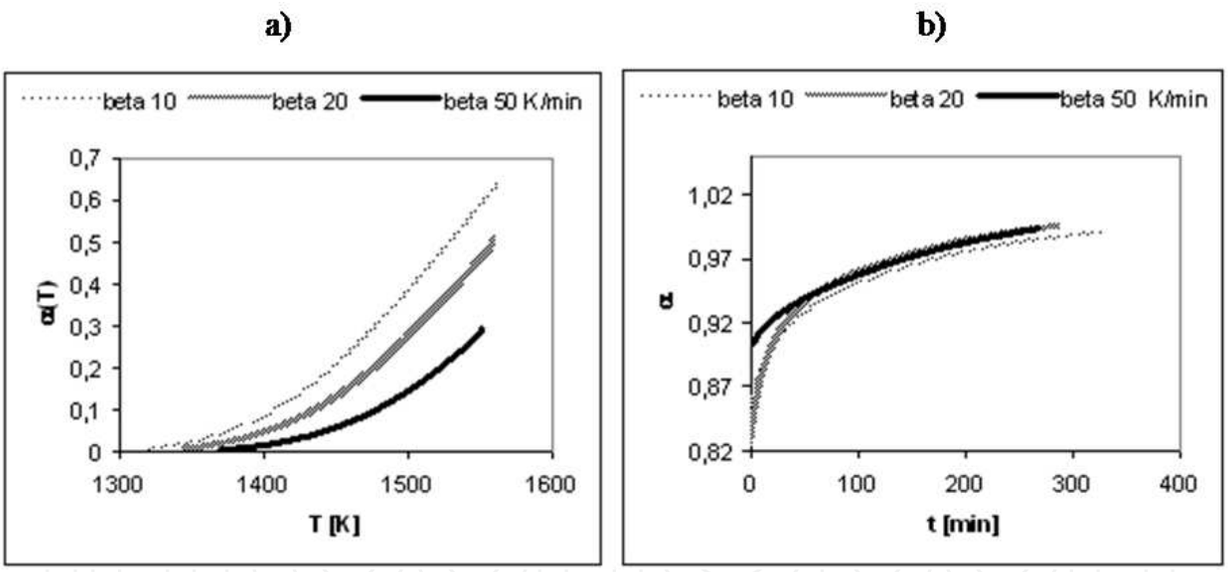

Figure 16. Conversion degree dependencies on temperature and time. Purification and carbonization of nc-TiC/C in argon. Stage II. a) non-isothermal conditions b) isothermal conditions.

The dependencies of α(T) determined for stages I, II and III under non-isothermal conditions, at a linear heating rate of the samples, were evaluated by neural networks method. The α(T) was the described variable and the sample heating rate and temperature were the describing variables. For each stage all the measurements series were analyzed simultaneously. The results are listed in Table 7

According to the theory of non-isothermal processes kinetics, the α(T) dependencies, determined for the stages, describe with high accuracy two parameters: sample heating rate

and sample temperature. These results could therefore be used in further calculations, i.e., during the identification of kinetic models (determination of the form of g(α) function)) and during determination of Arrhenius parameters A and E.

Parameter	Stage I , MLP 2/2			Stage II			Stage III, MLP 2/15		
	Tr	We	Te	Tr	We	Te	Tr	We	Te
S.D. Ratio	0.0361	0.0355	0.0364	0.0269	0.0274	0.0284	0.0728	0.0820	0.0784
Correlation	0.999	0.999	0.999	0.999	0.999	0.999	0.997	0.997	0.997

Table 7. Estimation of α(T) dependencies determined for stage I, II and III with use of artificial neural networks method.

First, the values of these parameters were estimated by linear regression method. Each series were analysed separately. The obtained results for stage III are given, as an example, in Table 8.

β [K/min]	r*	F	E [kJ/ mol]	A [1/min]	T_m [K]	$\Delta\alpha$	ΔT
10	-0,988	50029,7	315,09	8,48 E09	1530	0.005-0.639	1321-1564
20	-0,988	47245,7	327,77	3 E10	1559	0.005-0.508	1345-1560
50	-0,989	20219,0	375,62	1,95 E12	1590	0.004-0.29	1370-1551

Table 8. List of kinetic parameters. Stage III, model F1.
r* - correlation coefficient, F – Snedecor statistic

Using the determined values of A and E parameters, the values of α(T) were calculated from the Coats-Redfern equation. They were compared with the data determined from the measurements. The systematic error in the order of 4.5% has been noted. The accuracy was improved by correcting the value of E parameter. There was required that the error in the series, i.e. the mean square error between the values determined from the measurements and calculated $\ln\left[\frac{g(\alpha)}{T^2}\right]$, was close to zero. The calculations for the remaining stages were performed in the same way. The results are given in Table 9.

The results have been verified. Using the kinetic parameters given in Table 9 the conversion degrees were calculated from the Coats-Redfern equation for the e stages and compared to the ones determined from measurements. As an example, in Figure 17 the results for stage I are shown. A good consistency was obtained.

The kinetic parameters determined for the stages have been used for simulation calculations. The α(T) and r(α,T) dependencies on temperature and sample heating rate were investigated. The results are presented in Figure 18.

The determined dependencies are in accordance with the theory. With the increase in sample heating rates the α(T) curves are shifted into the higher temperature range. The

process rate increases from zero for α(T) equal zero, reaches the maximum in temperature Tm, and then usually decreases to zero at α(T)→1. The temperature ranges for stages runs are consistent with the ones determined experimentally. The α(T), and r(α,T) plots for a stage do not come to an end, because at high conversion degrees process ran according to the different kinetic models.

stage	Model	g(α)	β [K/min]	A [1/min]	E [kJ/mol]	T_m [K]	Δα	ΔT [K]
I	D3	$\frac{3}{2}\left[1-(1-\alpha)^{\frac{1}{3}}\right]^2$	10	2,2 E-6	15,8	487,4	0,03-0.9989	299-826
			20	1,2E-6	16,5	524,9	0,035-0,9969	299-937
			50	3,5E-7	16,3	539,5	0.005-0.9995	298-1319
II	F2	$(1-\alpha)^{-1}-1$	10	6,81 E4	125,25	1128	0.002-0.999	935-1271
			20	7,74 E6	160,8	1156	0.002-0.999	1007-1291
III	F1	$\left[-\ln(1-\alpha)\right]$	10	8,48 E09	306,8	1530	0.005-0.639	1321-1564
			20	3 E10	318,8	1559	0.005-0.508	1345-1560
			50	1,95 E12	364,5	1590	0.004-0.29	1370-1551

Table 9. List of kinetic parameters for the stages.

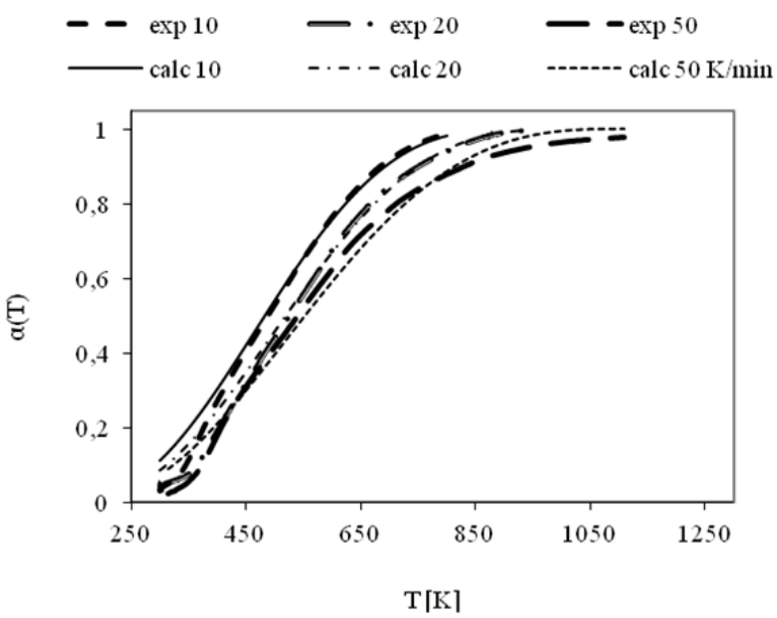

Figure 17. Comparison of α(T) calculated and determined from experiments. Stage I, model D3.

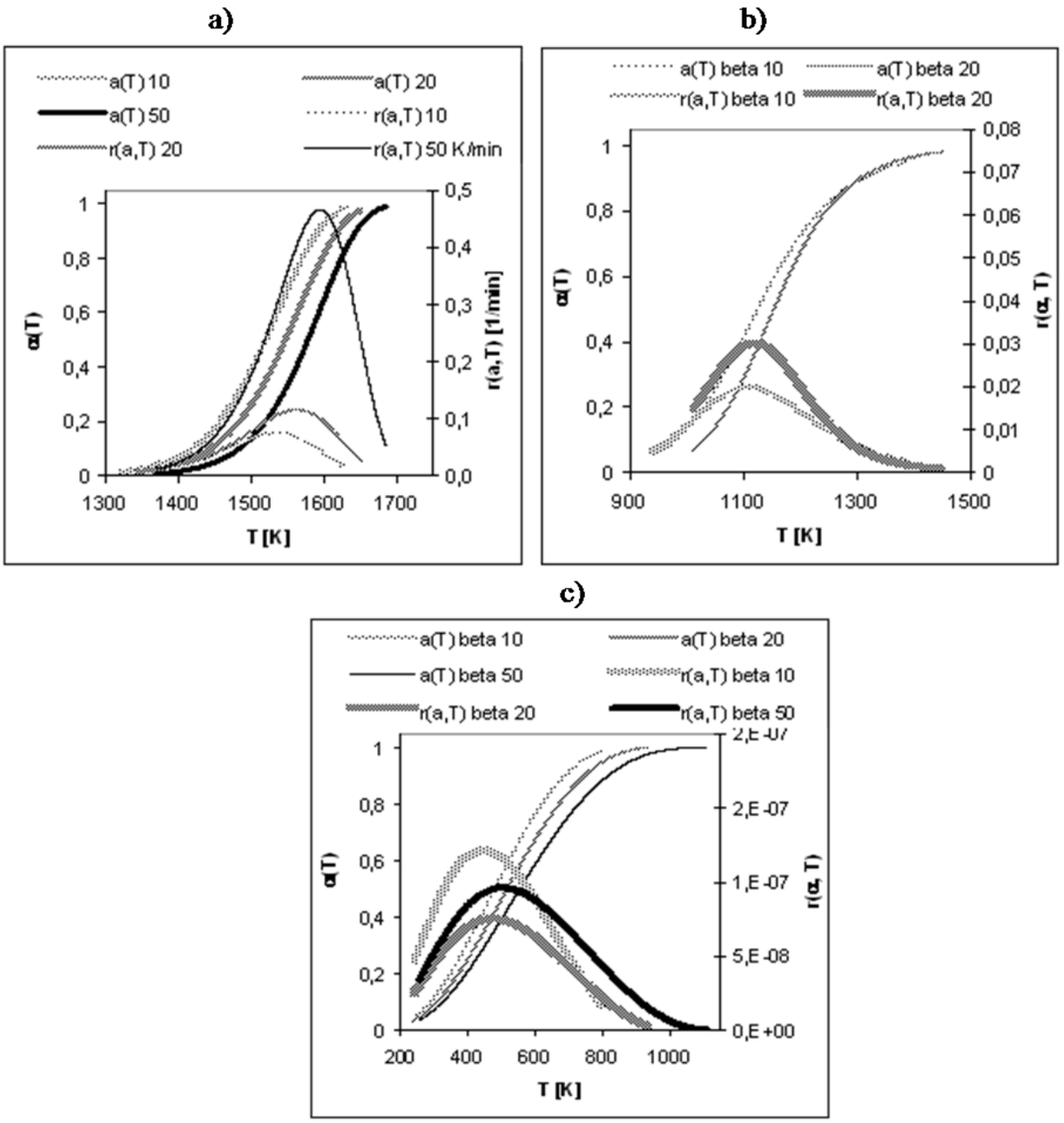

Figure 18. Plots of α(T) and r(α,T) functions; a) stage I, model D3; b) stage II, model F2; c) stage III, model F1.

Under the isothermal conditions the last phase of stage III and whole the stage IV proceeded. The results presented earlier, obtained in the series up to 1573, 1673 and 1773 K, were not sufficient for description of the course of stage III under isothermal conditions. They have been complemented by additional measurements. During the investigations samples were heated up to 1343, 1503, 1543 and 1623 K using the following heating rates: 10, 20 $Kmin^{-1}$.

While elaborating these results the calculations for stages I, II and III were also performed. There were obtained similar results as before (Table 9). These data are not provided. At the

high conversion degrees in stage III the change of kinetic model (form of g(α) function) took place. Under the isothermal conditions, at lower conversion degrees, the process first proceeded according to the F1 model (similarly as under the non-isothermal conditions), then at high conversion degrees (higher than 0.98) according to the D3 (three-dimensional diffusion Jander's model). This concerns the removal of remaining products of pyrolysis.

The charts of α (T) were obtained from about 25,000 measurement points for each case. The value of k(T) was calculated by linear regression method for the subsequent sets, each containing 1100 values of the g(α) function. The results were evaluated using several measures. The values of R^2 measure were determined. The calculation results for all measurement series are given in Table 5. The temperature, the mean values of k(T) determined for the entire sets, the time of obtaining the isothermal conditions t_1, counted from the beginning of the measurement, and the conversion degree α_1 obtained for this time are given.

series	β [K/min]	T [K]	k*10³ [1/min]	t_1	α_1	R^2
1443 K	10	1440,9	13,61	158,4	0,7092	99,72
	20	1440,9	14,41	99,98	0,69	99,92
1503 K	10	1501,1	14,75	203,92	0,9553	99,68
	20	1501	35,18	92,85	0,872	99,59
1543 K	10	1541,4	9,39	201,72	0,9331	99,72
	20	1541,3	12,48	142,69	0,9539	99,87
1573 K	10	1568,5	6,94	199,19	0,9303	99,36
	20	1568,2	8,3	131,15	0,938	99,85
1623 K	10	1620,2	40,63	162,6	0,9653	99,91
	20	1619,7	61,84	91,8	0,9615	99,95
1673 K	10	1669,4	54,28	160,2	0,9699	99,69
	20	1669,1	104,31	86	0,9883	99,39
1773 K	10	1770,5	219,28	154,2	0,9831	99,72
	20	1770	242,24	83,6	0,9831	99,52

Table 10. The results of kinetic calculations for isothermal conditions. F1 model.
R^2 – statistical measure

In the considered range of temperature two processes preceded simultaneously; pyrolysis of organic compounds, contained in the raw samples and proceeding with their participation carbonisation of nc-TiC_x/C. The bounded carbon remains in the system. As a result the lesser sample mass losses were observed. In lower temperature proceeds also pyrolysis, as shown by the values of k(T) given in Table 10. Carbonisation starts at temperature of about 1541 K and becomes a dominating process at temperature of about 1570 K. At 1610 K pyrolysis becomes a dominating process again. With regard to carbonisation effectiveness, the process should be carried out at temperature of about 1570 K. The minimum on the curve k(T) has been observed in Figure 19.

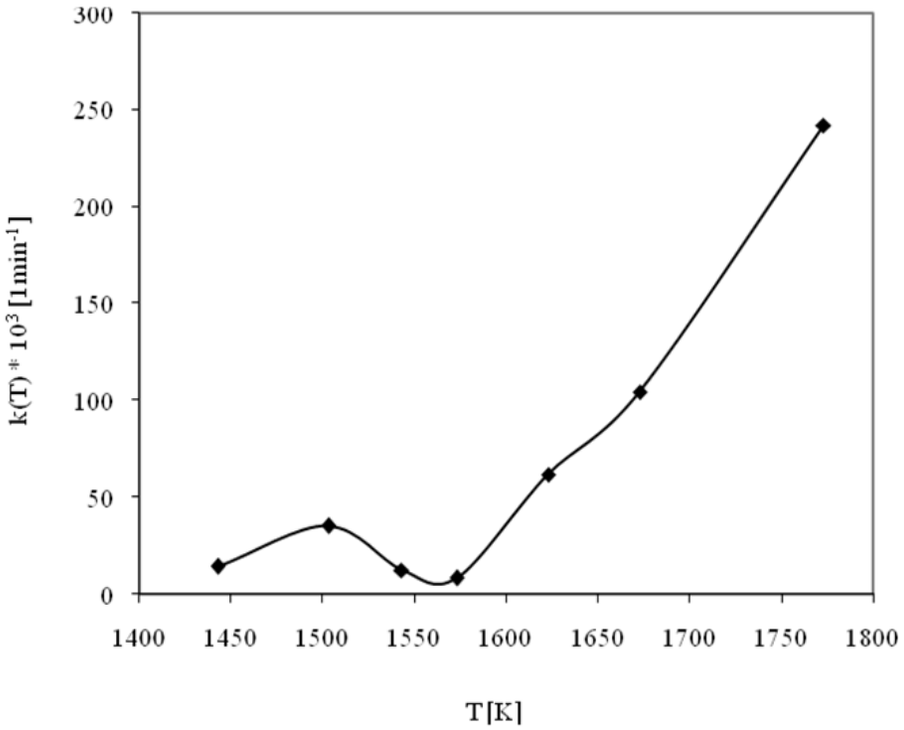

Figure 19. Dependency of reaction rate constant on temperature for β = 20 K/min. F1 model (g(α) = [-ln(1 - α)]); ♦– mean value of k(T)

In the same manner were obtained the results presented in Table 11, concerning the desorption process of volatile products after the completion of carbonisation process.

series	β [K/min]	T [K]	k*10³ [1/min]	t_2	α_2	R^2
1543 K	10	1541,4	0,255	402,3	0,989	97,82
	20	1541,3	0,354	326,2	0,9933	95,03
1573 K	10	1568,5	1,47	221,76	0,9412	99,59
	20	1568,2	2,34	150,98	0,9486	99,65
1673 K	10	1669,4	9,5	160,2	0,9699	99,69
	20	1669,1	16,07	87	0,9892	99,45
1773 K	10	1770,5	41,08	154,18	0,9831	99,66
	20	1770	49,36	84,1	0,9854	99,57

Table 11. The results of kinetic calculations for isothermal conditions. D3 model

In the third column the values of k(T) are given, and in the subsequent columns time t_2 from which desorption becomes the dominant factor, and the corresponding conversion degree.

Under the measurement conditions the oxidation of carbonised nc-TiC, by the oxygen contained in trace amounts in argon, occurred in series up to 1673 and 1773 K. This process proceeded according to the R2 model (reaction at the interface, cylindrical symmetry) or R3 model (reaction at the interface, spherical symmetry). The weight gain of the sample was less than 1%. Inhibition of oxidation process of carbonised nc-TiC can be explained on the

basis of the mechanism of Shimada [26], the formation on the surface of nc-TiC particles of amorphous TiO_2 layer, blocking access of oxygen to the reaction zone. The given values of k(T) indicate that the samples obtained at heating rates of 10 K/min oxidized slower than at the heating rates of 20 and 50 K/min. It is also visible that the final temperature of the process affects the properties of carbonised nc-TiC. Basing on the series up to 1673 and 1773 K there was found that after the completion of carbonisation and purification process of nc-TiC, at higher temperatures oxidation of the carbonised nc-TiC by oxygen present in argon in trace amounts takes place.

The removal of carbon from the matrix and carbonisation of nc-TiC_x proceeded most preferably in a series up to 1573 K, at the heating rate of 20 K/min. The results of investigations concerning this series are therefore given.

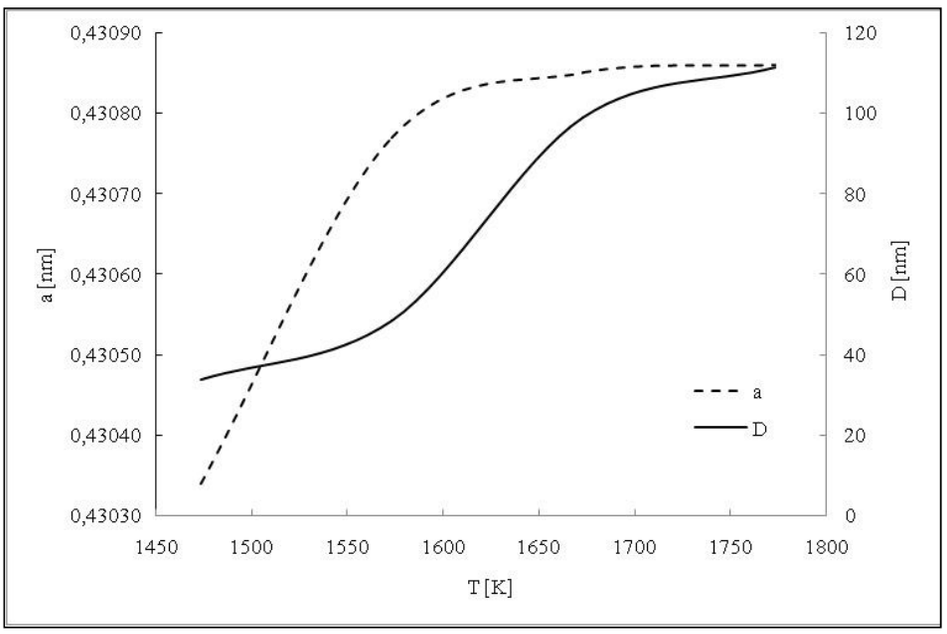

Figure 20. Dependency of nc-TiC mean lattice parameters (a) and mean particles diameters (D) on temperature [32].

Carbonisation resulted in an increase of lattice parameter of titanium carbide. The largest increase in lattice parameter was observed for the series up to 1573 K. Under these conditions, the average particle size was in the order of 40 nm. Mean values of lattice parameters of nc-TiC and the average particle size determined after the carbonisation processes are shown in Figure 20. The measurement of crystallites size by Scherrer method and on the basis of TEM images showed that the mean size of TiC crystallites after carbonisation was approximately 30% higher in relation to the size before the heat treatment process at temperature of 1573 K. The results of microscopic examination were confirmed by the results of the X-ray diffraction. The analysis of chemical composition and phase composition showed an increase in the fraction of carbon in titanium carbide from $TiC_{\sim .68}$ to $TiC_{\sim .8 \div .85}$ and removal of carbon from the matrix. The results of this step of research are given in [6,32].

4. Oxidation of the nc-TiC_x/C and nc-TiC_x

The possibility of implementing purification of TiC_x/C composites by burning out the elementary carbon, composing matrix, was considered. The results of oxidation of nc-TiC_x/C system have been presented. Oxidation of the TiC_x/C powders, being an intermediate product of sol-gel synthesis, and of the TiC_x powders obtained by reduction with hydrogen was investigated. The reduction of TiC_x/C powders with hydrogen aimed at removing from the system the carbon from the matrix. Purification with hydrogen according to the reaction $C+H_2 \rightarrow CH_4$ was carried out at temperature of 1173K, under pressure of 16MPa, for 4.5 h [6,32]. The measurements were carried out using thermogravimetric method, under non-isothermal conditions. The samples unreduced with hydrogen were studied at the following heating rates: 5Kmin^{-1} (sample weight of 18.749 mg), 10 Kmin^{-1} (sample weight of 16.049 mg), 15 Kmin^{-1} (sample weight of 13.322 mg), 20 Kmin^{-1} (sample weight of 15.908 mg). The powders after reduction with hydrogen instead were studied at 5 Kmin^{-1} (sample weight of 17.768 mg), 10 Kmin^{-1} (sample weight of 17.174 mg), 15 Kmin^{-1} (sample weight of 17.544 mg), 20 Kmin^{-1} (sample weight 17.544 mg). During the measurements temperature of samples, TG, DTG, and HF were recorded. In one series several dozen thousands of each variable values were recorded. During the measurements the linear change of sample temperature over time was maintained, as required by the theory of non-isothermal kinetics. The normalized TG curves of the samples unreduced and reduced with hydrogen are shown in Figure 21.

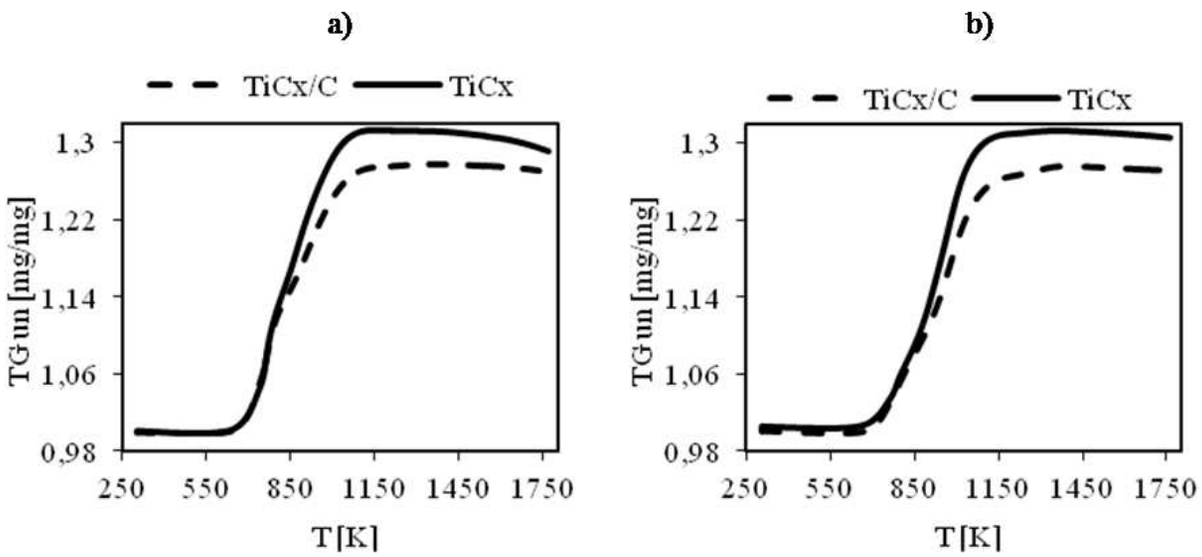

Figure 21. Plots of TG_u curves for TiC_x/C samples and TiC_x (after reduction with H_2) samples, a) 5, b) 20 Kmin^{-1}

The normalized TG_u curves of the samples reduced with hydrogen are shifted upward to the same degree for different heating rates (ΔTG in the order of 0.03 mg), because in the TiC_x powders (after reduction with hydrogen), the relative content of titanium increased as a result of removing elemental carbon by acting with hydrogen. This resulted in greater weight gain of TiC_x during the oxidation in comparison with TiC_x/C. In both cases the

weight gain of the sample started at temperature in the order of 600 K. This means that under these conditions the oxidation of nc-TiC_x started.

In the DTG curves, there are three peaks (Fig. 22). The first peak is associated with start of the oxidation of nc-TiC_x. The subsequent weight loss is associated with the burning out of the elemental carbon, produced during the oxidation of the nc-TiC_x. This process proceeds simultaneously with the further oxidation of nc-TiC_x. The next peak concerns the oxidation of unreacted nc-TiC_x. The elemental carbon, contained in nc-TiC_x/C samples unreduced with hydrogen, burns out in the final stage of the process.

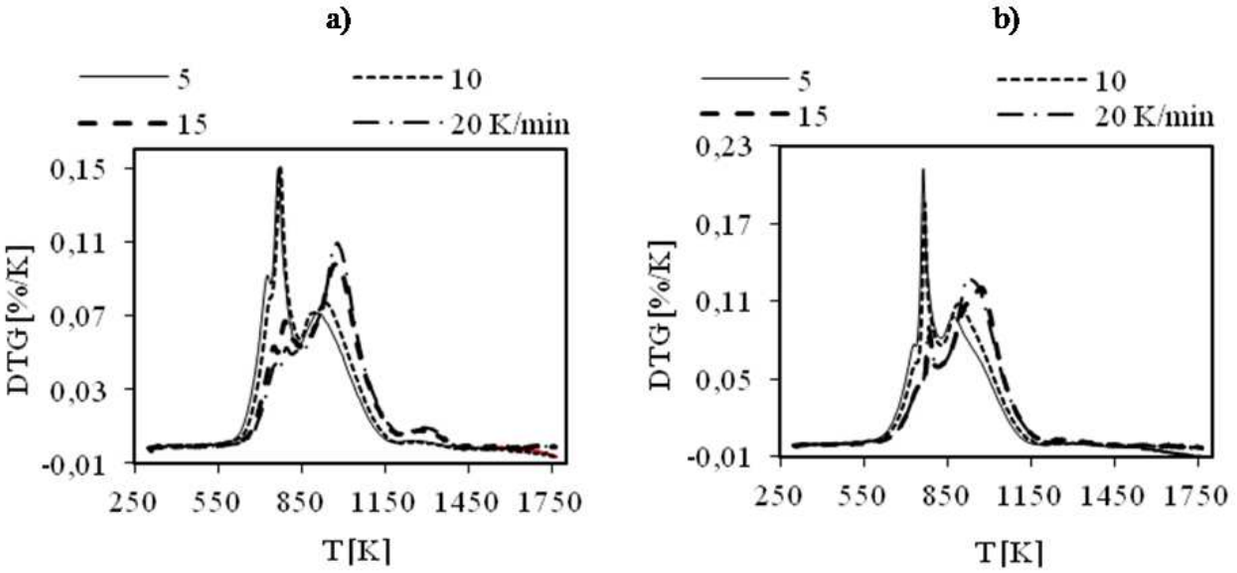

Figure 22. Dependency of DTG curves on temperature, a) for TiC_x/C, b) for TiC_x (after reduction with H_2)

Two distinct maxima were observed in the HF plots (Fig. 23). The first one is associated with the beginning of oxidation process of nc-TiC_x and the second one with burning out of the elemental carbon, produced during the oxidation of the nc-TiC_x, and further course of the nc-TiC_x oxidation. The apparent increase in the value of HF function, in the final stage of the process, is associated with the terminating oxidation of nc-TiC_x.

The results have been confirmed by the identification of CO_2, formed in the system, by mass spectrometry. There was also found that while increasing sample heating rates the plots of mass spectra of CO_2, originating from the nc-TiC oxidation process and from burning out of the formed carbon, overlapped. The carried out experiments have shown that the nc-TiC, obtained by sol-gel process, cannot be purified by burning out in the air the carbon admixtures contained in the system.

The performed studies indicated also the possibility of occurring during the description of oxidation of ceramic nc-TiC/C powders in the air, some difficult issue related to the simultaneous proceeding, in a certain range of temperature, of metal carbide oxidation and burning out of the carbon. The following manner of kinetics description of the both concurrent reactions, based on thermogravimetric studies, has been proposed.

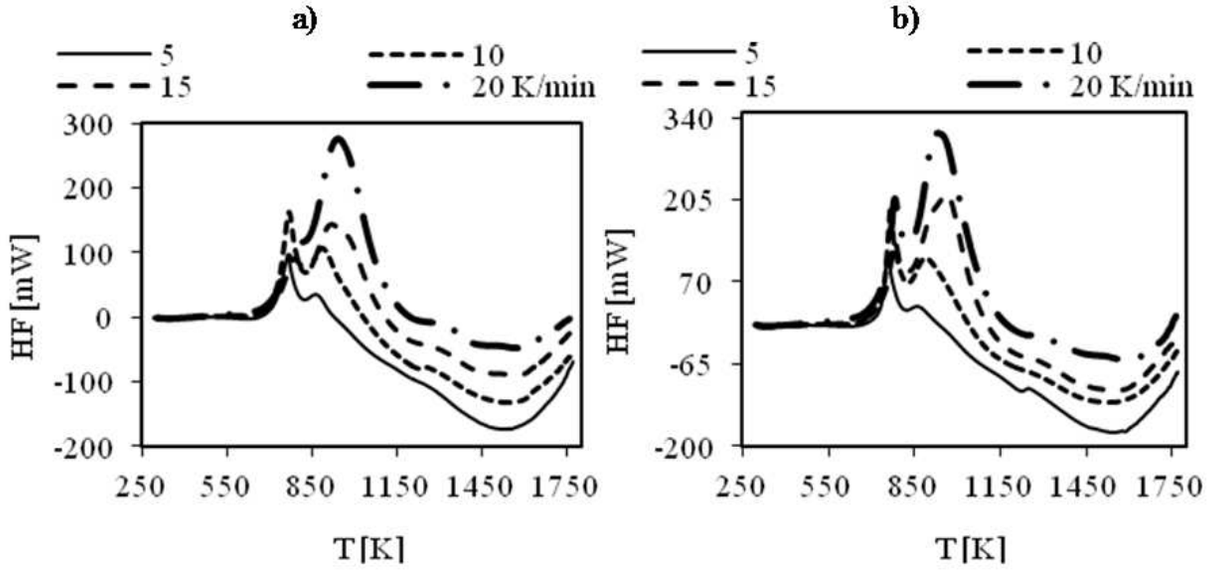

Figure 23. Dependency of HF on temperature, a) for TiC_x/C, b) for TiC_x (after reduction with H_2)

To obtain the normalized TG_u curve, corresponding to the oxidation process of TiC_x in the whole range of temperature the neural networks method was applied. Basing on the results registered before burning out of the formed carbon and after the end of this process the network was fitted. Then the fitted network was used to generate the segment of normalized TG_u curve for the temperature range in which both transformations proceeded simultaneously. The multi-layer MLP networks were used. The described variable was TG_u function, and the describing variable was temperature. Each measurement series was analysed separately. Using these models sections of TG curves corresponding to the oxidation process of nc-TiC, in the temperature range in which this process proceeded simultaneously with the burning out of the carbon, were generated. The TG_u plots generated by the network and determined experimentally are shown in Figure 24.

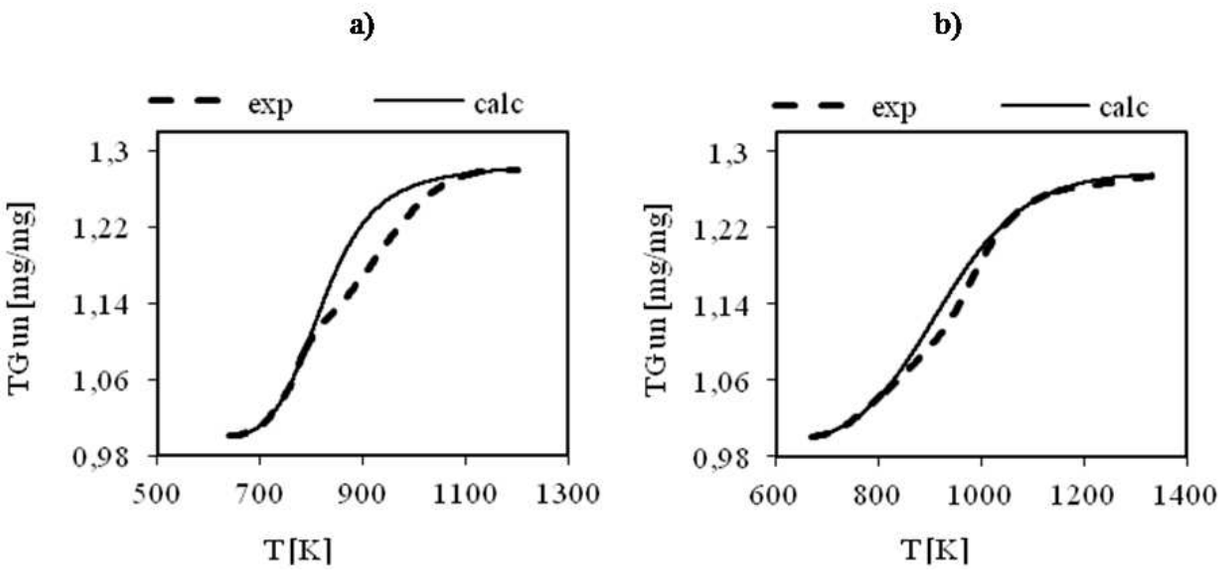

Figure 24. Plots of TG_u function, calculated and experimental. Oxidation of nc-TiC_x/C samples, unreduced by hydrogen, in air, a) 5 $Kmin^{-1}$, b) 20 $Kmin^{-1}$

On the basis of TG_u curves, complemented by the results of calculations, the α(T) dependencies for the oxidation process of nc-TiCx in the whole temperature range were determined.

The conversion degree for the process of burning out the elemental carbon was determined as follows. By subtracting the experimental values from the calculated TG_u values, ΔTG was determined, and then, integrating numerically, TG_u curves for the process of burning out the carbon were determined. The α(T) dependencies obtained for both processes, are presented in the form of graphs in Figure 25.

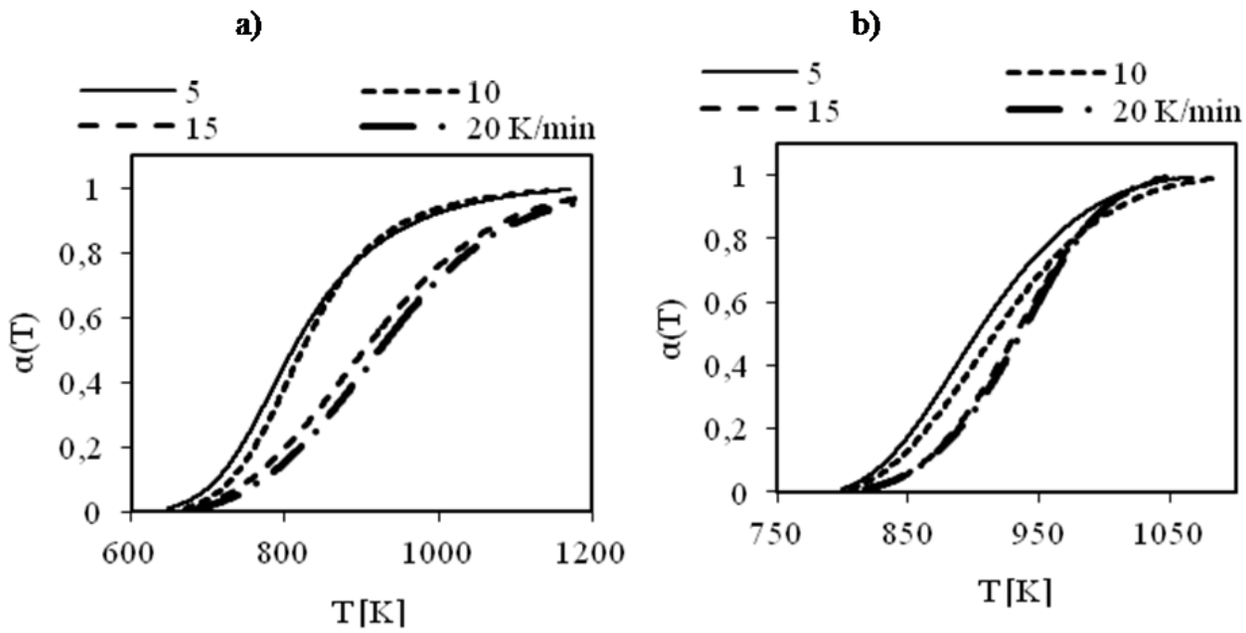

Figure 25. The α(T) dependencies. Oxidation of unreduced nc-TiC_x/C in air, a) oxidation of nc-TiC_x, b) burning out of elemental carbon

According to the theory, along with the increase in sample heating rates, the plots of α(T) are shifted into the higher temperature range.

The conversion degree for the process of burning out the carbon in the matrix (the second temperature range) was calculated in the same way. In the case of the oxidation process of nc-TiC_x (after reduction with hydrogen) two stages occurred: nc-TiC_x oxidation and burning out of the elemental carbon formed at the beginning of the oxidation process of nc-TiC. The α(T) dependence was determined for all the stages in the same way. The determined α(T) dependencies were the basis of kinetic studies. The Coats-Redfern equation was used. For all the stages kinetic models and Arrhenius parameters were determined (Table 12).

These data contain the full information about the kinetics of analysed processes. There should be noted that the kinetic parameters (the forms of g(α) functions and the values of A and E) determined on the basis of experimental data, should correspond to their physicochemical meaning. In the analysed case, the F2 model [$g(\alpha) = (1-\alpha)^{-1}-1$], having a theoretical justification, was used, and the determined activation energy values are similar to those found in many chemical reactions.

Sample	Conversion	Model	B [K/min]	A [1/min]	E [kJ/mol]	T_m [K]	$\Delta\alpha$	ΔT [K]
TiC_x/C	TiC	F2	5	26343,35	88,31	810,45	0,01-0,99	648-1147
			10	291522,00	99,20	822,77	0,01-0,99	671-1141
			15	16689,12	86,70	903,79	0,02-0,99	691-1245
			20	22863,39	89,26	923,22	0,01-0,99	690-1295
	$C_{elemental}$	F2	5	1,76E+10	185,04	902,35	0,02-0,99	803-1058
			10	8,27E+09	177,71	916,13	0,02-0,99	809-1085
			15	4,74E+12	222,13	932,37	0,02-0,98	827-1046
			20	7,1E+12	223,18	936,23	0,01-0,99	817-1042
	C_{matrix}	F2	15	5,24E+16	391,91	1243,06	0,02-0,98	1142-1366
			20	7,22E+16	392,43	1246,63	0,02-0,99	1138-1373
TiC_x after reduction	TiC	F2	5	1,01E+06	106,33	809,11	0,01-0,99	645-983
			10	1,37E+05	95,18	838,82	0,01-0,99	649-1134
			15	1,70E+05	98,51	892,95	0,01-0,99	673-1153
			20	3,19E+05	100,63	886,78	0,01-0,99	668-1144
	$C_{elemental}$	F2	5	6,98E+09	178,41	902,90	0,02-0,99	803-1063
			10	6,44E+09	174,85	908,97	0,02-0,99	810-1078
			15	1,55E+12	214,49	933,09	0,02-0,99	832-1063
			20	5,19E+11	204,20	930,08	0,02-0,99	830-1071

Table 12. List of kinetic data for the transformations in oxidation processes of titanium carbide samples before and after the reduction with H_2.

Basing on the obtained results an analysis of the process has been performed. The r(α,T) dependencies on sample heating rates and sample temperature for the stages were studied. The plots of r(α,T) obtained for the nc-TiC_x/C not-reduced with hydrogen are shown in Figure 26.

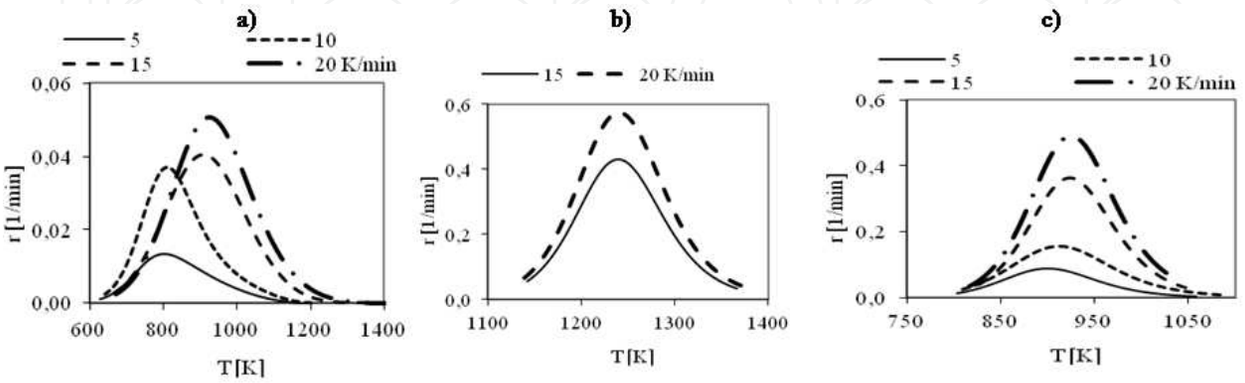

Figure 26. Plots of r(α,T). Oxidation of nc-TiC_x/C unreduced with hydrogen; a) oxidation of nc-TiC_x, b) burning out of the carbon formed during the oxidation process of nc-TiC, c) burning out of the carbon contained in the samples

According to the theory of kinetics of non-isothermal processes the reaction rate should increase along with the increase in sample heating rates. This condition is not well fulfilled for the oxidation process of nc-TiC_x unreduced with hydrogen (Fig.26a). This means that the samples used in measurement series differed. For the both processes of burning out the carbon the results consistent with theory were obtained. There should be noted that according to the theory, in each stage the process rate increases from zero for $\alpha(T)=0$, reaches the maximum in temperature Tm, and then decreases to zero at $\alpha(T)\rightarrow 1$. The temperature ranges determined for the stages runs on the basis of calculations are consistent with the ones determined experimentally.

The analogous plots obtained for the oxidation process in air of nc-TiC_x reduced with hydrogen are shown in Figure 27.

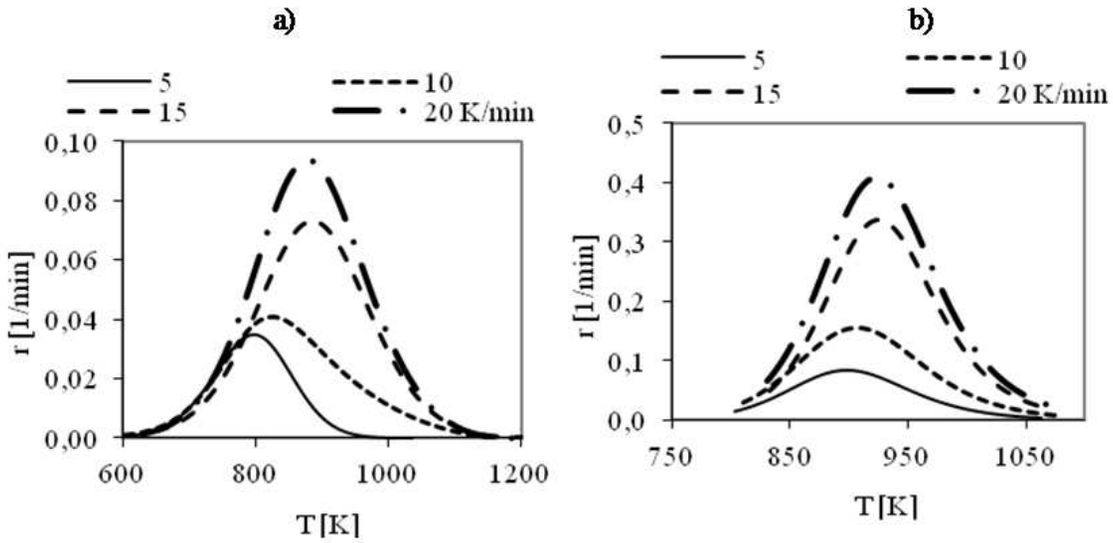

Figure 27. Plots of r(α,T). Oxidation in air of nc-TiC reduced with hydrogen; a) oxidation of nc-TiC_x, b) burning out of elemental carbon formed during the oxidation of nc-TiC_x

In this case, full consistency with the theory was obtained. The plots in Figure 27a show that nc-TiCx after reduction with hydrogen was uniform, the process rate increased along with the increase in sample heating rate, and the maximum was shifted into the higher temperature range. In both cases, the process rate, according to the theory, increases from zero for $\alpha(T)=0$, reaches its maximum at the temperature T_m, and then decreases to zero at $\alpha(T)\rightarrow 0$. The temperature ranges determined for the stages runs in measurement series on the basis of calculations are consistent with the ones determined experimentally.

The obtained results show that the proposed description method of the kinetics of two reactions proceeding simultaneously in a certain range of temperature, allows obtaining a satisfactory accuracy. This method was developed for the needs of processes of oxidation in air of nanocrystalline TiC and nanocomposites of TiC/C with varying carbon content in the matrix, for evaluating the protective qualities of carbon matrix, and also to evaluate and compare the resistance to oxidation of carbide ceramics [17]. In Figure 28 the use of the kinetics knowledge for comparative evaluation of the rate of TiC/C nanocomposite oxidation, depending on the carbon content in the matrix is shown as an example.

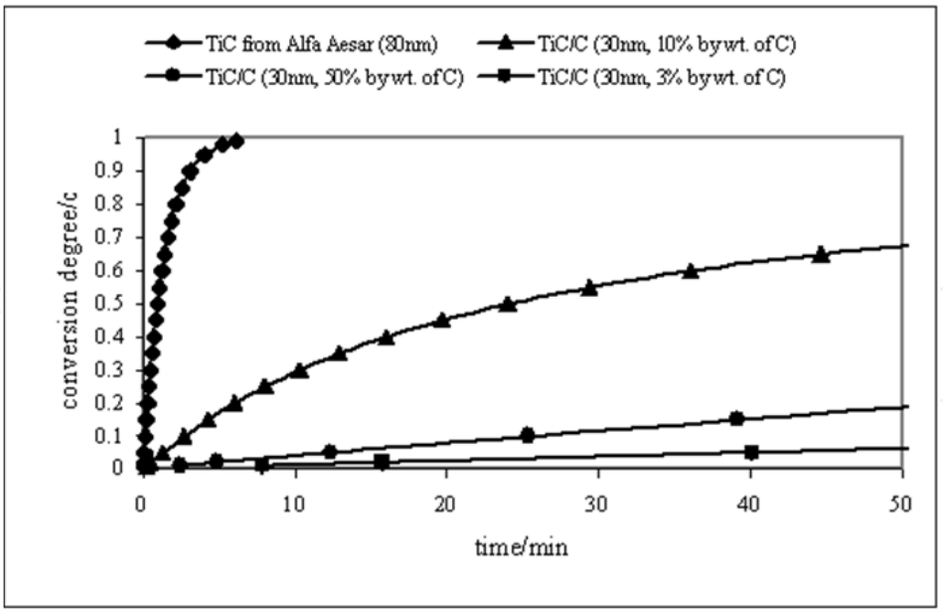

Figure 28. Dependence of conversion degree on time - α(t). T= 823 K. Oxidation of TiC commercial and TiC/C nano-composites (30 nm) in air. 50, 10, 3 % by wt. of the carbon contents in composites respectively [17].

5. Conclusions

The results of thermal decomposition of NH_4VO_3 in dry air have been presented. The measurements were carried out by TG – DSC method. The gaseous products were determined by MS method. Solid products were identified by XRD method. On the basis of measurement results the division of the process into stages has been made and the temperature ranges for stage courses and changes of sample masses in stages were determined. There was demonstrated that decomposition of NH_4VO_3 proceeds according to the following equation

$$6NH_4VO_3 \rightarrow (NH_4)_3 V_6O_{16} \rightarrow (NH_4)_2 V_6O_{16} \rightarrow 3V_2O_5$$

In all the stages at different sample heating rates NH_3, H_2O, NO and N_2O were evolved, which were formed as a result of NH_3 oxidation. NO_2 did not occur among the evolved gases. There should be added that N_2O was formed mainly during the stage II and III.

While performing the measurements the emphasis was placed on the possibility of obtaining experimental data for description of kinetics of investigated process, in accordance with ICTAC Kinetics Committee recommendations.

In the case of the investigated process, the necessary results for isothermal conditions were not obtained because the measurements for the stage could be performed only in a few temperatures, while at higher temperatures the results were obtained at high conversion degrees.

For non-isothermal conditions the needed data have been obtained. Kinetic calculations were performed using Kissinger's method, isoconversional method and Coats-Redfern method. Applying Kissinger's method the activation energies were determined and the

kinetic models were assigned for the stages. The stages I and III are well-described by model A2, and the stage II by model A4. It has been also shown that the influence of heating rate of the sample on the course of the process can be compensated, at constant activation energy, by temperature range $T_{\alpha=0} \div T_{\alpha=1}$, which is the value determined experimentally. The temperature ranges were given for the stages.

In case of the investigated process applying the isoconversional method the following results were obtained. The E values for the stages I and III (assimetric plots of DTG and HF) changed constantly along with the change of conversion degree. However, in the case of stage II (symmetric plots of DTG and HF), E was practically constant. It seems probable that the isoconversional method compensates the influence of β_i on the course of the process by changing the activation energy. Theoretically much more interesting is the possibility to compensate the β_i, at constant activation energy, with temperature range $T_{\alpha=0} \div T_{\alpha=1}$.

While carrying out the calculations using the Coats-Redfern method the activation energies determined by Kissinger's method were used as the base values. Almost constant values of the A and E parameters were obtained for the stages for different heating rate of the samples. The verifying calculations were performed. The $\alpha(T)$ and $r(\alpha,T)$ dependencies were determined. The good consistency with experimental data was obtained. The obtained results show that the Coats-Redfern equation is of great importance for the studies of the kinetics of heterogeneous non-catalytic processes

Describing kinetics of the TiC_x carbonisation and their oxidation, Coats-Redfern's equation was applied kinetic models of stages were identified based on statistical evaluation and compliance to a large extent, of degrees of transformation for stages calculated and determined from measurements. Building the kinetic models of processes, the results of measurements were treated as statistic values. A system of a complex analysis of measurements results was developed with the use of artificial neurone networks. Based on the TG curves four stages have been distinguished. The first, endothermic stage proceeding with mass loss, corresponded to desorption of volatile products, D3 model. The second, exothermic stage proceeding with mass growth, was assigned to oxidation of uncarbonized nc-TiC_x/C by the oxygen present in argon at trace level, F2 model. The third endothermic stage, proceeding with mass loss, referred to carbonization of nc- TiC_x/C and pyrolysis of organic compounds, contained in the raw samples. The pyrolysis of admixtures and carbonization of nc-TiC_x/C proceeded simultaneously. After completing the carbonization process at the temperature above 1573 K, oxidation of carbonized TiC_x/y by oxygen present in argon at trace level was observed, R2 model.

The third, basic stage preceded in non-isothermal and isothermal conditions; at lower conversion degrees F1 model (first-order reaction) and at the higher conversion degrees (above 0.98) D3 model (three-dimensional diffusion, spherical symmetry, Jander equation) was applied.

Adapting to the description of the processes which took place with the participation of nc-TiC_x/C the parameters for the process of purification were determined together with the simultaneous carbonization of nc-TiC_x in argon, in conditions which make impossible their

coalescence and growth to micron sizes. Kinetics and by the same, the mechanism of the processes of oxidation of nanocrystalline TiC_x in form of powder were tested, and they were subjected to evaluation based on the comparison of the rate of oxidation.

6. Nomenclature

GRNN	- Generalized-Regresion Neural Network
MLP	- Multilayer Perceptron
MS	- Mass Spectrometry
SEM	- Skanning Elektron Microscopy
TEM	- Transmission Electron Microscopy
TG – DSG	- Thermogravimtry and Differential Scanning Calorymetry
XRD	- X-Ray Diffraction
A	- pre-exponential Arrhenius factor ($1 min^{-1}$)
B	- const
C	- const
E	- apparent activation energy ($J\ mol^{-1}$, $kJ\ mol^{-1}$)
$f(\alpha)$	- conversion function dependent on mechanism of reaction
$f'(\alpha_m)$	- derivative of $f(\alpha)$ function for maximal reaction rate
$\phi(T, \alpha, P)$	- temperature, conversion degree and pressure function
$g(\alpha)$	- integral form of kinetic model
h(P)	- pressure function
k(T)	- reaction rate constant ($1\ min^{-1}$)
m_0	- initial sample mass for the stage (mg)
m	- current sample mass for the stage (mg)
m_k	- final sample mass after for the stage (mg)
r	- reaction rate ($1\ min^{-1}$)
R	- gas constant ($J\ mol^{-1}\ K$)
r_p	- correlation coefficient
t	- time (min)
T	- temperature (K)
$T_{\alpha=0}, T_{\alpha=1}$	- initial and final temperature of the stage (K)
T_m	- maximum conversion rate temperature for a stage (K)
$T_{\alpha'_m}$	- temperature referring to α'_m
ΔT	- temperature range (K)
TG_u, TG_{un}	- normalized TG
α	- conversion degree
α_m	- conversion degree for maximum rate of a stage
α'_m	- average conversion degree for rate maxima of a stage for different heating rate
$\Delta\alpha$	- conversion degree range
β	- heating rate ($K\ min^{-1}$)
Subscripts	
m	- maximum rate of a stage
i, j	- order

Author details

Anna Biedunkiewicz
Institute of Materials Science and Engineering West Pomeranian University of Technology, Szczecin, Poland

Acknowledgements

This work it concerns were partially generated in the context of the MULTIPROTECT project, funded by the European Community as contract No. NMP3-CT-2005-011783 under the 6th Framework Programme for Research and Technological Development. Financial support of part of the work by the Ministry of Science and Higher Education within the Projects No N N507 444334, 2008–2011 and No NR15-0067-10/2010-2013, is gratefully acknowledged.

The scientific support of my teacher professor Jerzy Straszko throughout this work is gratefully acknowledged.

7. References

[1] Vyazovkin S, Burnham AK, Criado JM, Perez-Maqueda LA, Popescu C, Sbirrazzuoli N (2011) ICTAC Kinetics Committee Recommendation for Performing Kinetic Computations on Thermal Analysis Data. Thermochimica acta, 520: 1-19
[2] Weimer AW, Nilsen KJ, Cochran GA, Roach RP (1993) Kinetics of carbothermal reduction synthesis beta silicon carbide. AIChE j. 39:493-503
[3] Chaudhurry S, Mukerjee SK, Vadya NV, Venugopal (1997) Kinetics and Mechanism of Carbothermal Reduction of MoO_3 to Mo_2C, J alloy comp. 261(1-2): 105-113
[4] Patel M, Subrahmanyam J (2008) Synthesis of Nanocrystalline Molybdenum Carbide (Mo_2C) by Solution Route. Mater research bulletin. 43: 2036-2041
[5] Wanjun T, Yuwen L, Xi Y, Cunxin W (2004) Kinetic Studies of the Calcination of Ammonium Metavanadate by Thermal Methods. Ing eng chem res. 43 (9): 2054-2059
[6] Biedunkiewicz A (2009) Aspects of Manufacturing of Ceramic Nanomaterials of TiC/C, TiC, TiC-SiC-C and Ti(C,N)-Si(C,N)-Si_3N_4 Type by Sol-Gel Method; Szczecin: West Pomeranian University of Technology, 177p.
[7] Liu CH, Li WZ, Li HD (1996) TiC/Metal Nacreous Structures and Their Fracture Toughness Increase, J. mater res. 11(9): 2231-2235
[8] Thorne K, Ting S, Chi CJ (1992) Reduction of Titanium Dioxide to Form Titanium Carbide. J. mater sci. 27: 4406-4414
[9] Koc R, Folmer JS (1997) Carbothermal Synthesis of Titanium Carbide Using Ultrafine Titania Powders. J. mater sci. 32(12): 3101-3111
[10] Lu Q, Hu J, Tang K, Deng B, Qian Y, Zhou G, Liu X (1999) The co-Reduction Route to TiC Nanocrystallites at Low Temperatures. Chem phys lett. 314(1-2): 37-39
[11] Burakowski T, Wierzchoń T (1999) Surface Engineering of Metals: Principles, Equipment, Technologies, New York: CRC Press, 592p.
[12] Ohring M (1992) The Materials Science of Thin Films, New York: Academic Press, Inc. Harcourt Brace Jovanovich Publishers, 704p.

[13] Voitovich VB, Laverenko VA (1991) Oxidation of Titanium Carbide of Differency Purity, Soviet metallurgy met ceram. 30 (11): 927-932
[14] Jin Y, Liu Y, Wang Y, Ye J (2010) Synthesis of (Ti, W, Mo, V)(C, N) Nonocomposite Powder From Novel Precursors. Int refract j hard mater. 28: 541-543
[15] Yeh CL, Wang HJ (2011) Combustion Synthesis of Vanadium Borides. J Alloys Compounds, 509: 3257-3261
[16] Mutin PH, Popa AF, Vioux A, Delahay G, Coq B (2006) Nonhydrolytic Vanadian-Titania Xerogels: Synthesis, Characterization, and Behavior in the Selective Catalytic Reduction of NO by NH_3. Applied catal b: environ; 69 (1-2): 49-57
[17] Biedunkiewicz A, Gordon N, Straszko J, Tamir S (2007) Kinetics of Thermal Oxidation of Titanium Carbide and Its Carbon Nano-composites in Dry Air Atmosphere. J therm anal cal. 88 (3): 717-722
[18] Burnham AK, Weese RK, Wernhoff AP, Maienschein JL (2007) A Historical and Current Perspective on Predicting Thermal Cookoff behavior. J therm anal calorim. 89: 407-415
[19] Biedunkiewicz A, Gabriel U, Figiel P, Sabara M (2012) Investigations on NH_4VO_3 Thermal J therm anal cal., 108:965–970
[20] Coats AW, Redfern JP (1964) Kinetic Parameters From Thermogravimetric Data. Nature, 201: 68-69
[21] Vyazovkin S, Wight CA (1999) Model-Free and Model-Fitting Approaches to Kinetic Analysis of Isothermal and Nonisothermal Data. Thermochim acta, 340-341: 53-68
[22] Biedunkiewicz A, Strzelczak A, Chrościechowska J (2005) Non-isothermal Oxidation of TiCx Powder in Dry Air. Pol j chem technol; 7 (4): 1-10
[23] Biedunkiewicz A, Strzelczak A, Możdżeń G, Lelątko J (2008) Non-isothermal Oxidation of Ceramic Nanocomposites Using the Example of Ti-Si-C-N Powder: Kinetic Analysis Method, Acta mater. 56: 3132-3145
[24] Straszko J., Biedunkiewicz A, Strzelczak A (2008) Application of Artificial Neural Networks in Oxidation Kinetic Analysis of Nanocomposites, Pol j chem technol, 10(3):21-27
[25] Galway AK (2003) What is Mean by the Term "Variable Activation Energy" when Applied in the Kinetic Analyses of Solid State Decompositions (Cryptolysis Reaction)? Thermochim acta, 397:249-268
[26] Shimada S, Kozeki M (1992) Oxidation of TiC at Low Temperatures, J mater sci. 27: 1869-1875
[27] Shimada S (2002) A Thermoanalytical Study on the Oxidation of ZrC and HfC Powders with Formation of Carbon. Solid state ionics, 149 (3-4) : 319–326
[28] Shimada S (1996) A Thermoanalytical Study on Oxidation of TiC by Simultaneous TG-DTA-MS Analysis, J meter sci. 30:673-677
[29] Shimada S (2001) Interfacial Reaction on Oxidation of Carbides with Formation of Carbon, Solid state ionics, 99: 141-142
[30] Shimada S (2001) Formation and Mechanism of Carbon-containing Oxide Scales by Oxidation of Carbides (ZrC, HfC, TiC), Mat sci forum 369-372: 377-384
[31] Gozzi D, Montozzi M, Cignini PL (1999) Apparent Oxygen Solubility in Refractory Carbides, Solid state ionics 123: 1-10.
[32] Biedunkiewicz A (2011) Manufacturing of Ceramic Nanomaterials in Ti–Si–C–N System by Sol–Gel Method, J sol-gel sci technol. 59: 448-455